The Geochemistry and Impacts of Chemical Weathering on the Central Namib Desert Gravel Plains Soils

Undergraduate Research Thesis
Submitted in partial fulfillment of the requirements for graduation
with research distinction in Earth Sciences
in the undergraduate colleges of
The Ohio State University

By

Caitlin Monagle
The Ohio State University
2020

Approved by

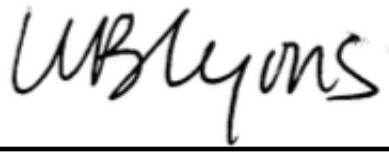

W. Berry Lyons, Advisor
School of Earth Sciences

TABLE OF CONTENTS

ABSTRACT

The Namib Desert is one of the most arid deserts in the world. Surficial soil samples were collected along a transect at 20 km intervals from Walvis Bay, on the Atlantic Coast, to 200 km inland where the transect ends. The focus of this study was to evaluate the accumulation of salts in the soils and to determine the extent of chemical weathering along the transect. The soils were leached with water for 5 days and the leachates were analyzed for concentrations of their major cations and anions. In addition, the solids were analyzed for their total major element concentrations. From 20 km to 90 km inland, the soils have higher concentrations of weatherable Ca and Na than do the samples inland. From 100 km to 200 km inland, these concentrations decrease. The chemical index of alteration (CIA) was determined using the results from the solid soil analysis. From 20 km to 140 km inland, the soils showed little to no weathering. From 160 km to 200 km inland, the soils were much more altered with the loss of major cations, Ca, Na, K. When combined, all these data clearly demonstrate the influence of precipitation on the geochemistry of the soils. The soils that are closer to the shore have a higher salt accumulation, whereas further away from the coastline there is a lower amount of salt accumulation indicating chemical weathering is occurring. These data support the general notion that there is a greater accumulation near the coast because there is less precipitation and causing the soils to have little to no weathering.

ACKNOWLEDGEMENTS

I would like to give a huge thank you to Berry Lyons for his mentoring and patience throughout the project. Also thank you to Sue Welch, Melisa Diaz, and Chris Gardner for their analysis, advising, and patience throughout the process. I am extremely grateful to Professor Don A. Cowan and his students and colleagues at the Centre for Microbial Ecology and Genomics, University of Pretoria, South Africa for collecting and sharing with me and WBL's research group the samples used in this study. Thank you to Anthony Lutton for his help with running the samples on the ICP-OES. Thank you to the McKenzie Brecher Undergraduate Scholarship for providing the funding to send the samples to the SGS Canada, Inc. lab for XRF analysis. The ICP-OES analyses was conducted by the Trace Element Research Laboratory (TERL), School of Earth Science, The Ohio State University. Thank you to the Edmund M. Spieker Memorial Scholarship, Joseph and Marcia Newhart Scholarship, and School of Earth Sciences Field Experience Travel Fund for providing funds that gave me the ability to attend the SES Field Camp in the summer of 2018. Thank you to my high school vocational teacher, Terry Regan, for inspiring me to become a geologist, for letting me to share my adventures throughout my undergraduate career with you, and for your wisdom through the years. I would like to thank my fellow Earth Science majors for making Ohio State my home away from home. I would like to thank Dr. Anne Carey for helping me get involved in research. I would like to thank Jen Mogensen for helping me become a better writer throughout the years, and for helping me finish this thesis when the odds were stacked against me. Finally, I would like to thank my family and my friend, David Aarons, for always being there for me through every struggle. I could not have made it through college without you.

LIST OF FIGURES

LIST OF TABLES

INTRODUCTION

The Central Namib Desert is one of the most arid deserts in the world. The desert has been arid for the past 130 million years (Viles and Goudie, 2013). The Central Namib Desert is composed of gypcrete, like many arid deserts around the world that form under conditions where more evaporation occurs than does precipitation (Watson, 1985). Deserts are classified based on the ratio of evaporation to precipitation which is also called aridity (Watson, 1985). Most arid desert gypsum crust forms in areas that have less than 250 mm of annual precipitation (Watson, 1985). The Namib Desert's gypsum crust is composed of both deserts rose crust and a bedded crust (Watson, 1985).

The Atacama Desert is another arid desert that is very similar to the Namib Desert climatically. The Atacama Desert is located along the coast of southern Peru and northern Chile, and between the central Andes (Rech, et. al., 2003). Off the coast of the Atacama in the Pacific Ocean upwelling occurs that forms marine aerosols that are deposited in the soil causing the accumulation of sulfate (Rech, et. al., 2003). The gypsum soil in the Atacama is composed of nitrate, chloride, and sulfate salts in which the coastal fog provides a source of the salts within the first 50 km of the coastline (Rech, et. al., 2003). As the Atacama increases in elevation and distance from the ocean, there is an increase in weathering of the bedrock because there is more moisture and precipitation (Rech, et. al., 2003). At the higher elevations in the desert, the soil accumulates salt through the evaporation of groundwater at the surface. This evaporation creates more salt which decreases the amount of weathering that occurs (Rech, et. al., 2003). The weathering processes that occur in the Atacama are similar to those in the Central Namib Desert.

The Central Namib Desert's weathering processes and sources of moisture have been studied extensively. The two major weathering processes the occurs in the study area are caused by the occurrence of coastal fog and rainfall events. In the Atlantic Ocean there are cold upwelling cells along the coast that cause coastal fog that has high humidity while preventing rain from occurring (Eckardt, et. al., 2012). The fog tends to stay near the coast and only extends about 60 km inland. The coastal fog is limited by the increasing elevations in the desert, like the coastal fog of the Atacama Desert (Eckardt, et. al., 2012). Ocean upwelling causing the marine aerosols to moves inland and then accumulate in the soils providing a major source of sulfate and calcium (Eckardt and Schemenauer, 1998).

The rainfall events in the Central Namib Desert are variable with each year and tend to have an average precipitation between 0 mm to 250 mm. Unlike the Atacama, when there is rainfall in the Central Namib Desert, some most of the soluble salts such as nitrate are dissolved which can cause a depletion in salts (Viles and Goudie, 2013). The rainfall varies temporally and spatially across the Namib Desert depending upon the atmospheric and sea surface temperatures (Eckardt et. al., 2012). The amount of precipitation tends to increase going from the coastline to the interior of the desert (Eckardt, et. al., 2012). The coastline typically receives less than 10 mm, but the interior of the gravel plains receives more than 50 mm (Eckardt, et. al., 2012). See Figure 1.

The overall goal of this research was to determine the geochemistry of the Central Namib Desert soils and how the soil geochemistry varies with aridity. It was hypothesized that as the distance from the Atlantic coast increases, the samples will progressively become more chemically weathered.

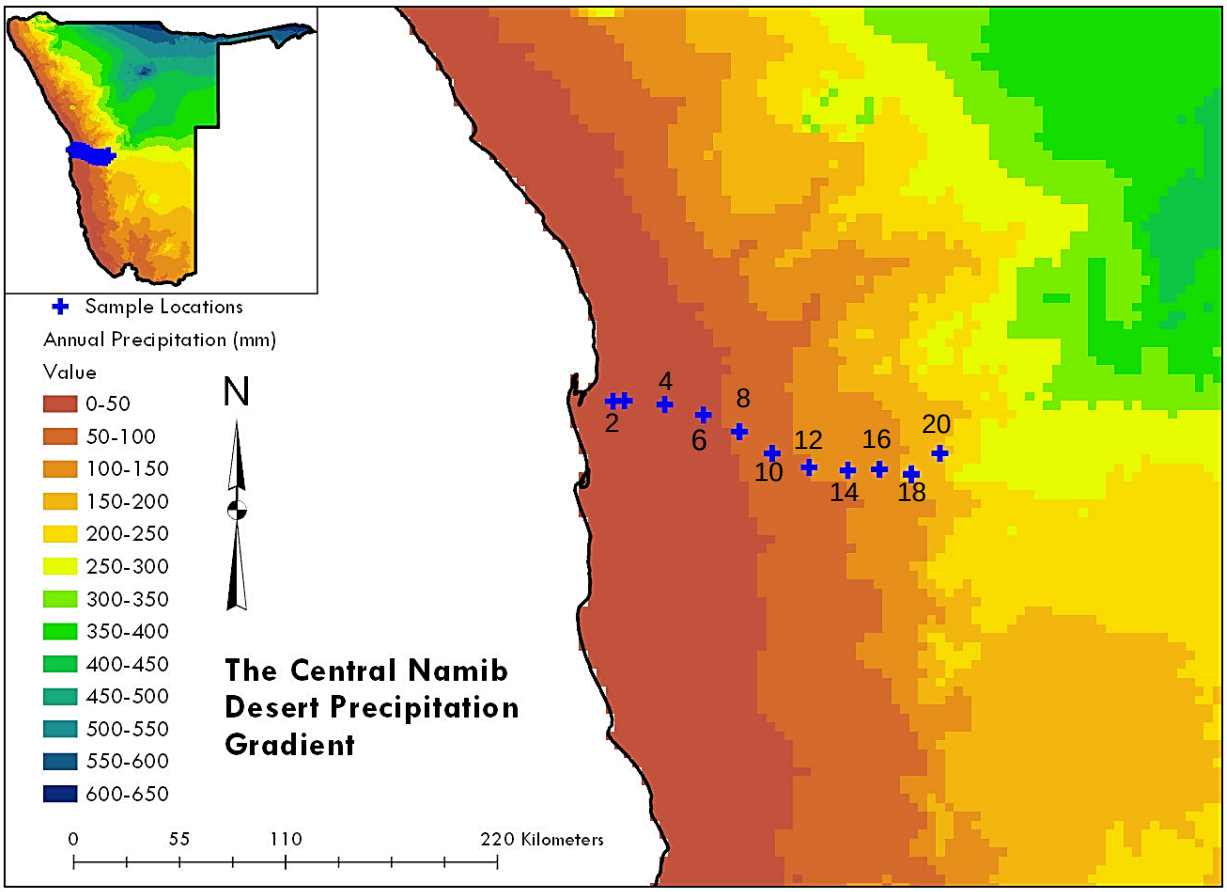

Figure 1. The Central Namib Desert precipitation gradient. The sample location are shown in the blue crosses.The map shows the mean annual precipitation in the study area location (Frick and Hijmans, 2017). The sample locations have precipitations ranging from 0 mm to 250 mm. The blue crosses denote the sample locations. The first sample location (location 2) is the blue cross closest to the coastline. See Appendix A for the sample location and information.

GEOLOGIC SETTING

The underlying geology in the study area were a result of the Damara Orogen that created the two of the major rock formations in the Neoproterozoic (Prave, 1996). The Kuiseb formation is composed of rocks that have been metamorphized and are of the amphibolite facies grade. The Kuiseb Formation is composed of the Matchless Amphibolite Belt, graphitic schists, marble, calcsilicate rocks, tremolite schists, scapolite schists, and meta-turbidites (Dombrowski et. al., 1996). The other major formation in the study area is the Donkerhoek Granite (Dombrowski et. al., 1996). The study area was originally thought to be a convergent continental setting before undergoing the Pan-African Damara Orogen (Dombrowski et. al., 1996).

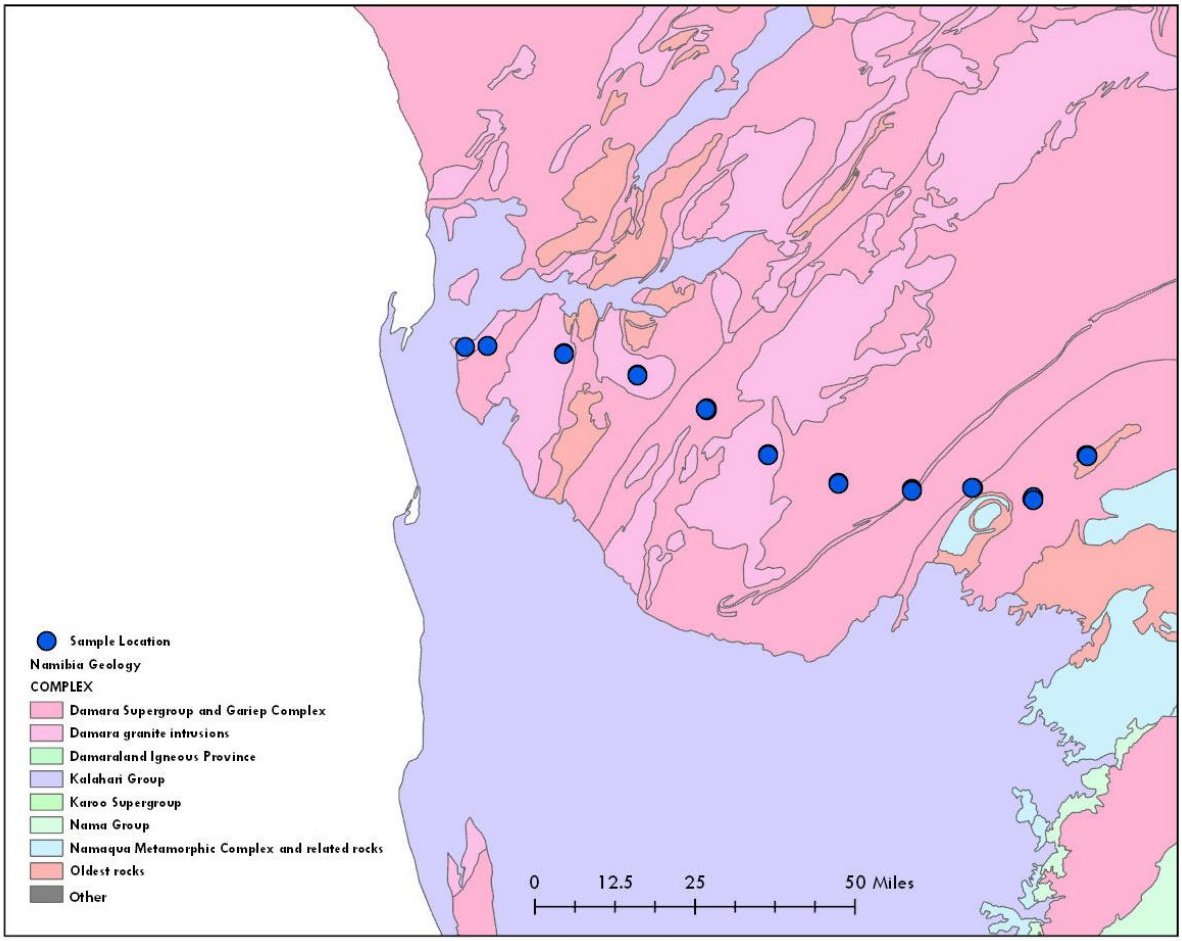

Figure 2. Geological Complex in relation to sample location (Ministry of Environment and Tourism, 2003).

METHODS

The soil was collected during April, 2017 along C14 and C26 public roads starting at Walvis Bay. The samples were collected in 20 km intervals going from east to west at 10 separate sites. The transect was chosen due to the varying rainfall, fog events, and changes in temperature. There were four replicate samples (~500 g) collected aseptically at each site from depth of 0 - 3 cm. Samples were collected by Professor Lyons' colleague, Professor Don Cowan and his students from Centre for Microbial Ecology and Genomics, University of Pretoria, South Africa.

Figure 3. Sample site photographs taken by Professor Don Cowan and his students in April of 2017. Picture A was taken at sample location 2. Picture B was taken at sample location 14. Picture C was taken at sample location 20.

Leaching Methodology

Before leaching, 5 g of the soil was weighed using a top loading balance and was put into the clean polyethylene falcon tubes. The polyethylene falcon tubes were then filled with 20 g of deionized water and were leaching for 5 days intervals. The sample was then filtered through 0.4 μm pore-size cellulose acetate membrane filters using deionized water rinsed nylon filtering apparatus. Some of the samples had to be filtered twice because particles passed through the initial filter. In between filtering the samples, and the filtration equipment was rinsed with deionized water. A new membrane filter was used while the old ones were discarded.

ICP-OES Preparation and Precision

Due to the very large variation in the water-soluble salt content of these soils, it was necessary to dilute some samples more than others in order to get concentrations of ions that fell within the range of our standards. All the samples were diluted at 10x when the samples were first analyzed. The samples that did not fall within the range of standards of the first sample run were then diluted to 2x or 100x (Table 1). The samples that were diluted at 100x were measured as saturated in Na during the first sample run. There were three types of dilutions that were created. The 10x dilutions consisted of 1 mL of sample, 0.2 mL of reagent grade HNO_3, and 8.8 mL of deionized water. The 100x dilutions consisted of 0.1 mL of sample, 0.2 mL of reagent grade HNO_3, and 9.7 mL of deionized water. The 2x dilutions consisted of 5.0 mL of sample, 0.2 mL of reagent grade HNO_3, and 4.8 mL of deionized water. The dilutions were prepared by first pipetting the water into the 10mL polypropylene falcon tubes. Then HNO_3 was added via pipette under a fume hood. Finally, the sample was added under the fume hood by using a new pipette

tip every time to ensure there was no cross-contamination. The precision of the ICP-OES is shown in Table 2.

Table 1. ICP-OES Dilutions

2X Dilutions	10X Dilutions	100X Dilutions
6A	2A	4C
8B	2B	8A
10A	2C	8D
10B	2D	
12A	4A	
12B	4B	
16A	4D	
16B	6B	
16C	6C	
16D	6D	
18A	8C	
18B	10C	
18C	10D	
18D	12C	
20A	12D	
20B	14A	
20C	14B	
20D	14C	
	14D	

Table 2. Accuracy and precision of analytical measurements. Accuracy was determined by analyzing NIST 1643e. Analytical precision was determined by calculating the RSD of the six replicates of a 0.5 mg/L calibration standard analyzed over the course of the analytical session.

Analyte	NIST 1643e Certified Concentration (mg/l)	NIST 1643e Result (mg/L)	Certified/Result (%)	Precision RSD (%)
Na	20.74	22.3	7	1.7
Mg	8.037	7.45	8	0.5
K	2.034	2.35	14	0.6
Ca	32.3	30.4	6	1.5
Sr	0.323	0.319	1	0.6
Ba	0.544	0.564	4	0.7

Ion Chromatography (IC) Procedure

There were standardized solutions that were analyzed to compare to the samples. The autosampler vial tubes were filled with 5 mL of sample. Data from the 10x dilution helped determine which sample needed further dilution. Anion samples were only diluted at 2x and 25x. For 25x dilutions, there were 0.2 mL of sample and 5 mL of deionized water that was pipetted into the vials (Table 3). If there was insufficient sample remaining from previous analyses, those

samples received a 2x dilution. For a 2x dilution, 2.5 mL of sample and 2.5 mL of deionized water were pipetted into the sample. Every tip that was used to pipette the sample was discarded to ensure each was used only once to avoid cross-contamination.

Table 3. IC Sample Dilutions

25x Dilutions	2x Dilutions
6A	20D
6B	16D
6C	
6D	
8A	
8C	
8D	

Samples were analyzed for the anions Cl^-, SO_4^{2+} using techniques outlined in Deuerling et. al. (2014). Bicarbonate was determined by the differences of the sum of the cations in equivalents (Na, K, Ca, Mg) minus the sum of anions in equivalents (Cl^-, SO_4^{2+}) as described in Deuerling et. al. (2014).

Table 4. IC Concentrations of C14-14D in μg/g and Precisions (n=1)

Analyte	Concentration and Precision
F	0.02 ± 0.00
Cl	14.155 ± 0.425
Br	0.055 ± 0.015
NO_3	0.135 ± 0.015
PO_4	0.08 ± 0.00
SO_4	9.52 ± 0.19

Nutrient Analyzer Methodology

The samples were analyzed on the Scalar San ++ Nutrient Analyzer. The analyses were conducted with methods supplied by the manufacturer and the techniques described in Deuerling et. al. (2014).

Table 5. Nutrient Analyzer Average Concentration in μg/g and Relative Standard Deviation (n=32).

Analyte	Average Concentration and Relative Standard Deviation
Si	13.1 ± 0.23
NO_3+NO_2	49.1 ± 5.35
PO_4	0.96 ± 1.14
NH_4	0.64 ± 1.99

XRF Procedure

The samples were sent to SGS Canada Inc. for analysis during the fall of 2018. The lab passed them through 180 μm mesh filter and then the samples were dried at 60°C and weighed. Major oxides were determined on 0.5 g sample after LOI was measured on a different, 1 g aliquot of the same sample. The 0.5 g samples were prepared via borate fusion and the beads analyzed by x-ray fluorescence techniques. Minor and trace metals were determined on the sample bulk, dried and sieved samples by either ICP-AES or ICP-MS after multi-acid digestions. Specific test details and accreditation of SGS Mineral Services Canada are available at http://www.scc.ca/en/programs/lab/minerals.html. Only one set of samples were analyzed in duplicate and the rest of the samples were only analyzed once. To access the precision of the major oxide measurements, sample C14-16B was analyzed twice. The precision of the major oxides measurements are shown in Table 6.

Table 6. Concentrations C14-6B and Precisions of the Major Oxide Elements (n=2)

Analyte	Concentration and Precision of Duplicate Measurements (%)
LOI	5.43 ± 0.15
SiO_2	68.6 ± 0.2
Al_2O_3	11.8 ± 0.1
Fe_2O_3	5.34 ± 0.03
MgO	2.06 ± 0.01
CaO	1.92 ± 0.00
K_2O	2.22 ± 0.01
Na_2O	1.69 ± 0.01
TiO_2	1.22 ± 0.01
MnO_2	0.10 ± 0.00
P_2O_5	0.08 ± 0.00

Table 7. Precisions of minor and trace elements data was determined by replicate analysis of sample C14-4A. All concentrations in μg/g.

Analyte	Concentration and Precision
Cs	3.0 ± 0.0
Rb	103 ± 1
Tl	0.57 ± 0.01
U	5.64 ± 0.56
Th	52.3 ± 2.6
Pb	24.1 ± 0.0
Ba	407 ± 1
Ce	172 ± 9
Ta	1.57 ± 0.02
Hf	3.4 ± 0.03
Zr	99.2 ± 7.8
Sr	186 ± 1

Nb	18.0 ± 0.5
Y	33.4 ± 1.2
Yb	2.5 ± 0.1
Ca	16.3 ± 0.6
Co	10.9 ± 0.1
Cr	82 ± 0.0
Ni	16.9 ± 0.1

Data Analysis

The Chemical Index of Alteration (CIA) is used to determine how much a sample has been weathered. The equation that was used to calculate the CIA from Nesbitt and Young (1982):

$$CIA = \frac{Al_2O_3}{Al_2O_3 + CaO + Na_2O + K_2O} \times 100$$

To graph the spider diagrams (Gaillardet et. al., 1999), the final values used in the graph were calculated from taking the values of the sample divided by the values of the upper continental crust from Rudnick and Gao (2003) and Dombrowski et. al. (1996). The elements were ordered in stability using Gaillardet et. al. (1999) and Dombrowski et. al. (1996).

RESULTS

Anion Concentration

Figure 4 show that the average anion concentration increased and reached the highest concentration around 80 km inland from the Atlantic Coast, but then decreased as the sample transect progressed further inland.

The general pattern of SO_4^{2-} is decreasing with distance from the Atlantic Coast (Figure 4). SO_4^{2-} had the highest concentration around 60 km and 80 km inland. Around 190 km inland there was a sample that was lower in concentration than the samples from approximately at 60 km, 80 km, and 120 km.

Chloride has the highest concentration at about 120 km inland. The chloride concentrations of sample 8A (9.49×10^3 μg/g) and sample 8C (1.68×10^4 μg/g) are very high whereas sample 8B (5.4 μg/g) and sample 8D (6.5 μg/g) are very low concentrations. The samples from locations are replicate samples that are all 85 km away from the coastline. Chloride has a decreasing concentration as the samples progress further away from the coastline. Chloride had a lower concentration at about 170 km and 190 km relative to the samples taken closer to the coastline.

The highest concentration of nitrate occurs in sample 8C and is the only sample that has a concentration over 1500 μg/g, which is extremely high compared to the other soils.

Bromide exceeded 1 μg/g at 120 km and 80 km relative to the rest of the samples in the transect. The rest of the samples in which bromide was detected, the concentrations of the samples were low, the lowest being 0.1 μg/g. The sample with the lowest concentration of bromide occurred around 170 km. The fluoride concentrations never exceeded 1 μg/g.

Fluoride had the lowest concentration around 100 km. The numerical values of the anion concentrations are tabulated in Appendix A.

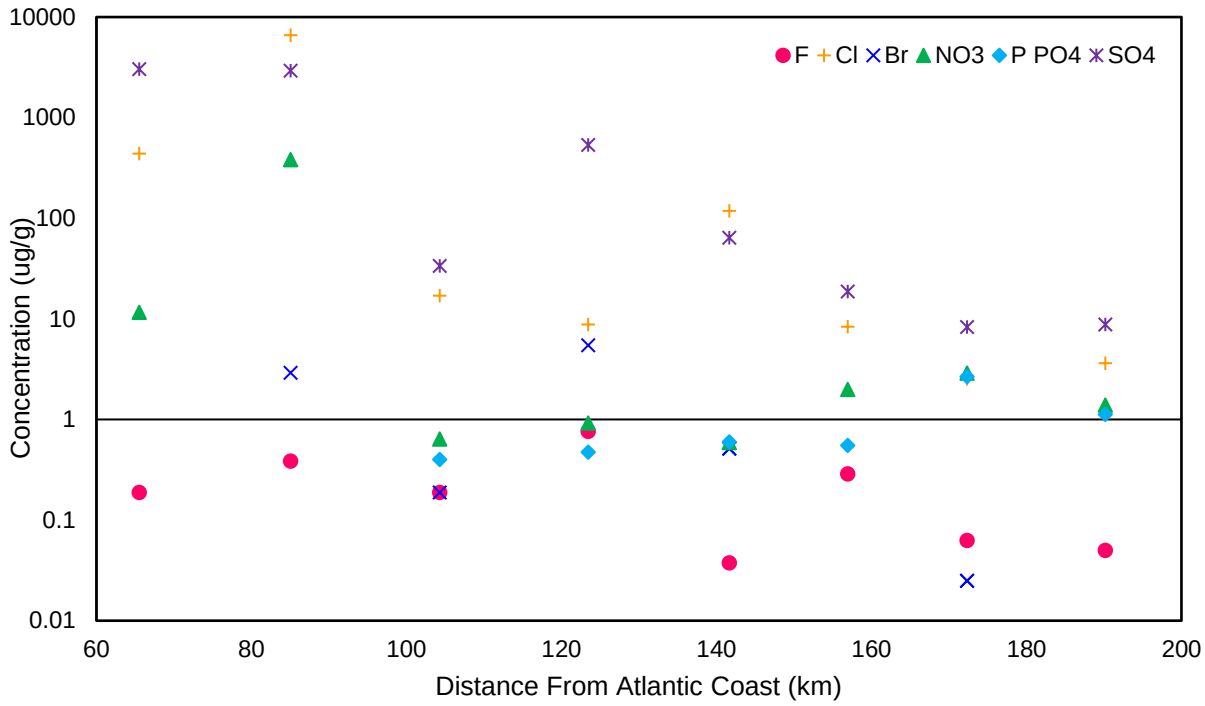

Figure 4. Average concentrations of anions in relation to the distance from the Atlantic coast.

Nutrient Concentrations

Figure 5 shows that the water-soluble silica concentration remained relatively constant regardless of the distance from the coast, with a range of concentrations between 10 μg/g and 20 μg/g. The lowest concentration of silica was observed in the sample taken at 170 km from the coast with a concentration of 10.66 μg/g. The highest concentration of silica is located about 120 km from the shore with a concentration of 17.08 μg/g.

Nitrate + nitrite (N+N) reached the highest concentration around 80 km inland. The concentration of nitrate + nitrite decreases in the middle of transect at 100 km inland with a value of 0.95 μg/g. The lowest concentration of nitrate + nitrite occurs at 140 km inland at 0.490 μg/g. The concentration of nitrate + nitrite slightly increases at the end of the transect at 190 km.

The concentrations of PO_4 increase as the transect progressed inland. The highest concentration of PO_4 is 3.11 μg/g around 170 km. NH_4 increases moving inland. The highest concentration of NH_4 occurs about 140 km inland, with a concentration of 1.16 μg/g. The lowest concentration of NH_4 is located at 65 km inland with a concentration of 0.011 μg/g. The nutrient concentrations are tabulated in Appendix B.

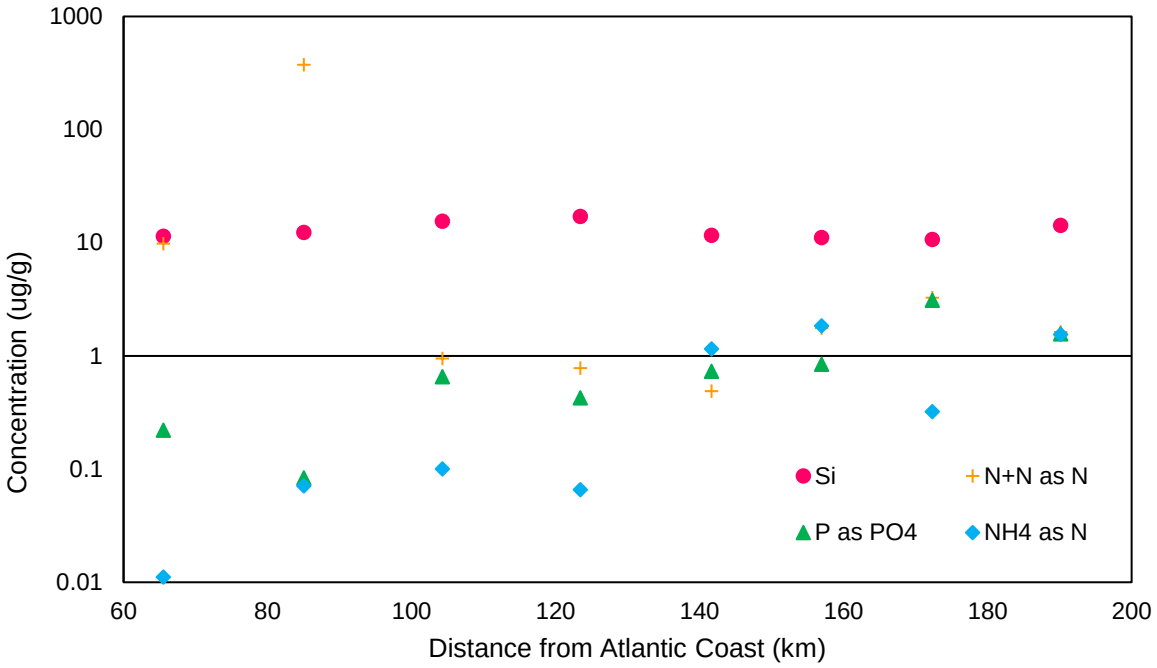

Figure 5. Average concentration of nutrients in relation to the distance from the Atlantic coast. The average concentrations were calculated from four replicate samples.

Cation Concentrations

Figure 6 shows that Ca, Na, Mg, K and Sr concentrations generally decreased as the samples advance further from the coastline. Mg had concentrations that were never below 1 μg/g, but never exceeded 20 μg/g. Mg had concentration concentrations ranging 1–20 ug/g at 155 km from the coastline. Na had concentrations slightly higher than 1 μg/g around 170 km and 190 km. Around 80 km, Na was significantly higher than the rest of the measurements along the transect. Ca and K were higher relative to the rest of the cations throughout the entire transect. Both Ca and K had their highest concentration at about 80 km. Ca had higher concentrations than K throughout the whole transect. Strontium had its highest concentration, 6.76 μg/g at 80 km.

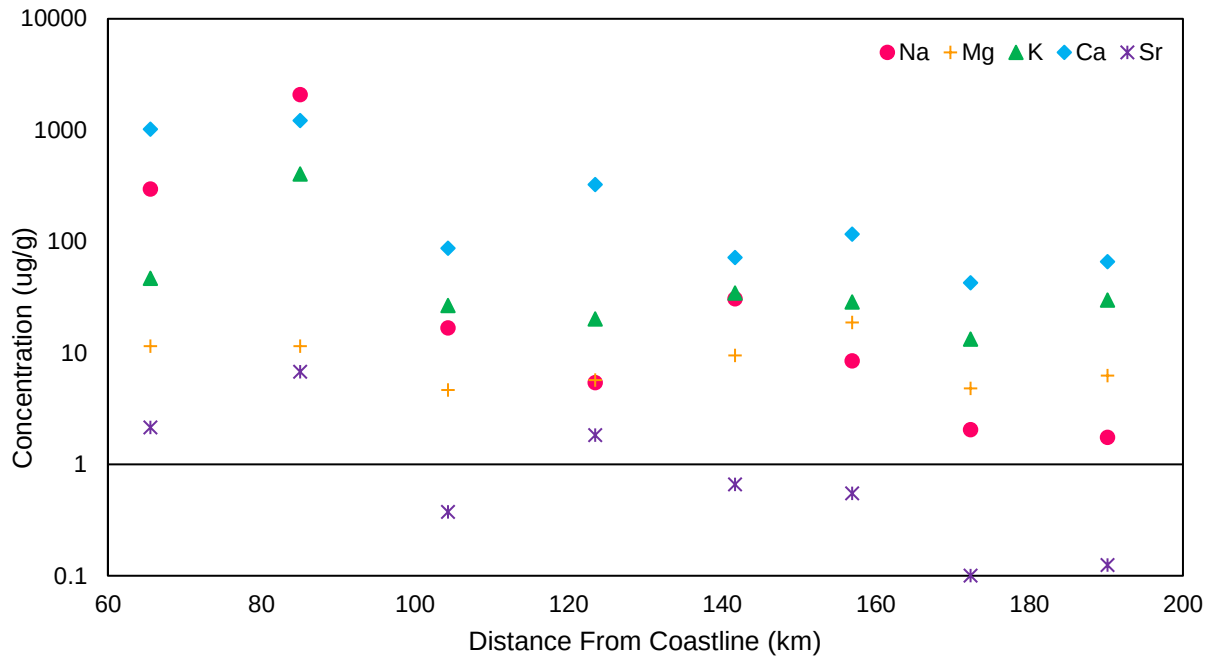

Figure 6. Average concentration of cations in relation to the distance from coastline.

Ternary Diagrams of the Water-Soluble Salt Data

In order to establish the relationship of the major soluble salt ion distribution among these soil samples, Ternary or Piper Diagrams were constructed. Figure 7 is a ternary diagram comparing the various cation concentrations in units of % mole ranging from 0% to 100%. Figure 8 shows that most of the samples range 0-40% of Mg. Two of the samples from location 8 have less than 20% Ca but are more than 80% enriched in Na+K. Most of the samples from location 6 contain less than 20% of Na+K, and more than 80% Ca. The samples from location 10 have a concentration of Ca of 40–80% and have a concentration of Na+K of 20-60%. Location 12 has a concentration of Ca of 60–100% and a concentration of Na+K of 0–40%. Most of the samples from location 14 had concentrations of both Ca and Na+K of 40–60%. The only sample that is an outlier from location 14 has a concentration of Ca of 60–80% and a concentration of Na+K of 20-40%. The samples from location 16 were about 60-80% Ca and 10–40% Na+K. Most of the samples from location 18 were 60-80% Ca and 10–35% Na+K. The other sample from location 18 was 20–40% enriched with Ca and was 40-60% enriched with Na+K. The samples from location 20 were 40-80% enriched in Ca and 20-40% enriched in Na+K. These data can be summarized in the following way; that samples 6, 10, 12, 16, 18, and 20 are enriched in Ca while sample 14 is moderately enriched while sample 8 is low in Ca. The sample 8 is close to the transition between 0–50 and 50–100 mm of precipitation. This transition maybe in some way related to the lower Ca values.

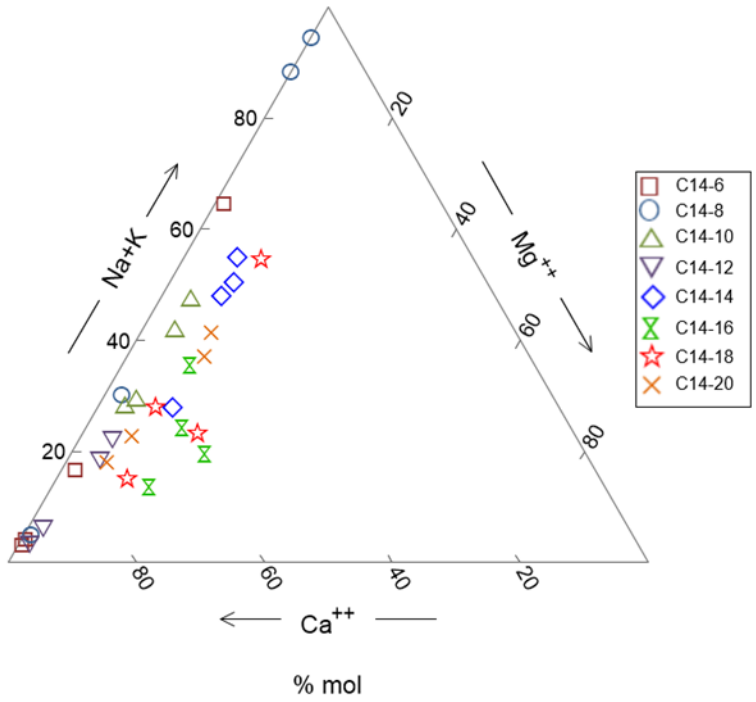

Figure 7. Tertiary diagram of cation analysis grouped by the sample location. Each location has 4 replicate samples and was designated a symbol based on location.

Figure 8 shows that most of the samples from location 6 were more than 80% enriched in SO_4 and had less than 20% of NO_3 and Cl. The samples from location 8 varied in SO_4 and Cl but had less than 20% NO_3. The samples from location 10 also varied in SO_4 and Cl and had 0–40% NO_3. Many of the samples from location 12 had more than 80% SO_4 and less than 20% NO_3 and Cl. Most of the sample from location 14 had less than 20% NO_3 and SO_4, but had more than 80% Cl. Sample location 16 varied in NO_3 and SO_4 and had 40–60% Cl. Sample location 18 varied greatly in NO_3, SO_4, and Cl. Location 20 had a concentration of Cl and SO_4 that ranged between 20-60%, but varied in NO_3.

These data can be summarized in the following manner; at increasing distance from the ocean there is a transition from a sulfate dominated system to soils more enriched in chloride. The highest soluble nitrate values are observed in samples 16, 18, and 20, and may reflect a biological source due to a higher precipitation rate.

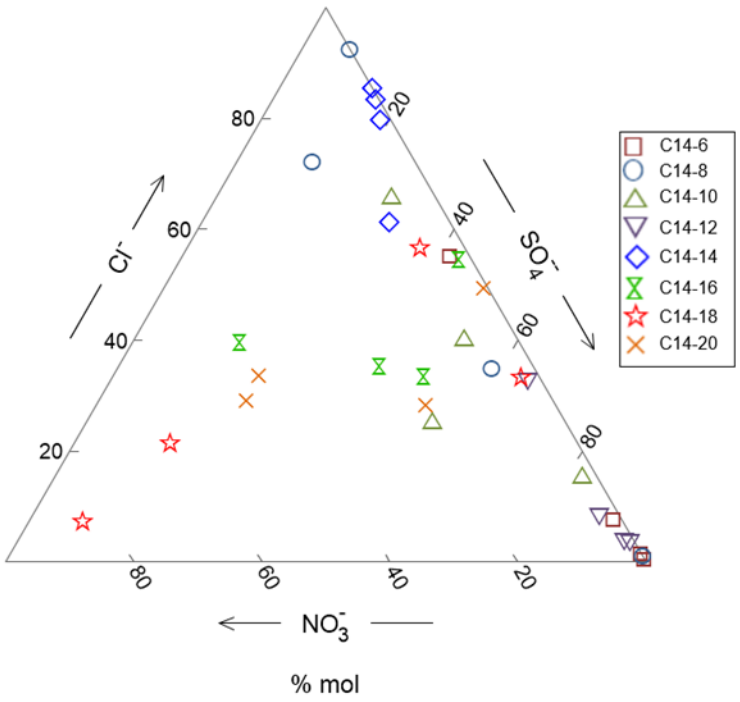

Figure 8. Tertiary diagrams of anions analysis grouped by the sample location.

Total Soil Elemental Composition

The results from one replicate sample from each location in the transect were analyzed via XRF and normalized against the upper continental crust (UCC) data from Rudnick & Gao (2003) (Figure 9). The elements and major oxides that were depleted relative to the UCC in all samples were Tl, Ba, K_2O, Hf, Sr, Zr, Na_2O, Co, Al_2O_3, and Ni. All samples were enriched in Th, Ba, and TiO_2 relative to the UCC. The only samples that were enriched in Cs were 2A, 4A, and 6B. The samples that were enriched in U were 14A, 16B, 18A, and 20B. The samples that were enriched in Nb, Yb, Y, Tb, and Lu were 2A, 4A, 6B, and 10A. Most of the samples were enriched or slightly enriched in La, Ce, and Ta. From 80 to 150 km the samples were depleted in Rb. The samples that were depleted in CaO were 8B, 16B, 18A, and 20B.

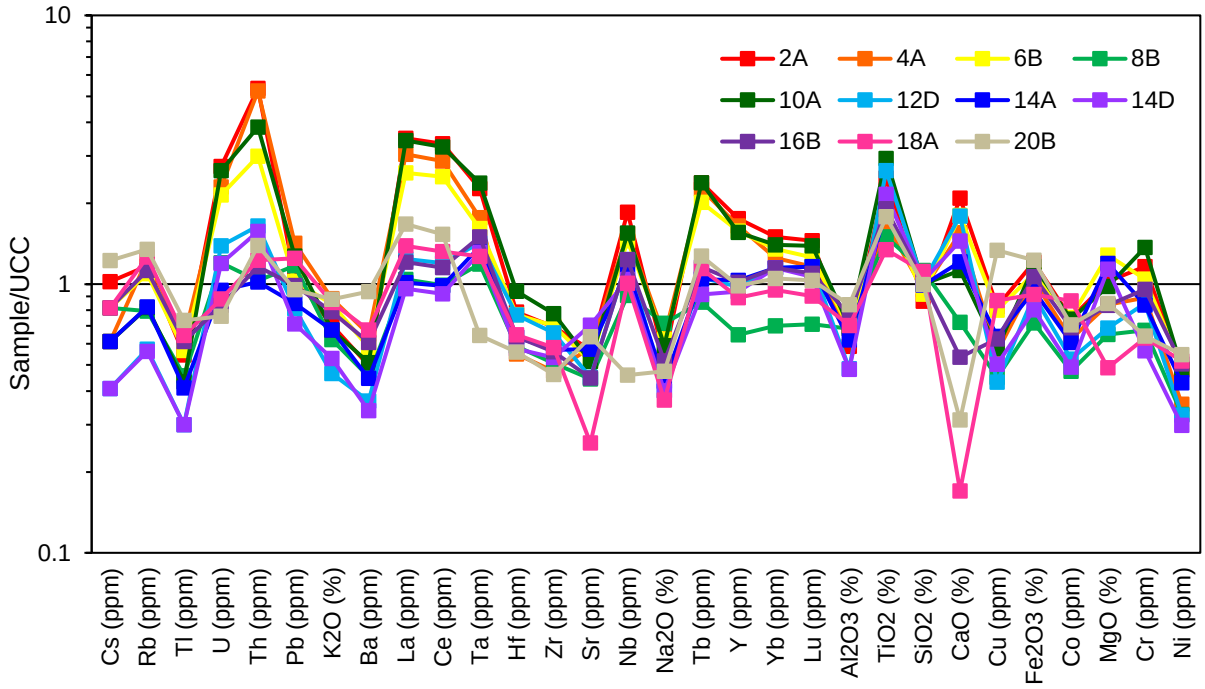

Figure 9. Spider diagram of sample concentrations normalized against the Upper Continental Crust with elements arranged in the order of stability.

The samples were normalized against Kuiseb Formation from Dombrowski et. al. (1996) (Figure 10). All samples were depleted in Rb, K_2O, Zr, Y, Al_2O_3, Co, MgO and Ni. All samples were enriched in TiO_2 and Fe_2O_3. The last sample in the transect 20B at 190 km inland was the only sample that was enriched in Ba. The rest of the samples were depleted in Ba. The only sample that was slightly depleted in SiO_2 was 2A which was slightly below 1. The rest of the samples were enriched in SiO_2, and they were all above 1. From 150 km to 200 km, the samples were depleted in CaO.

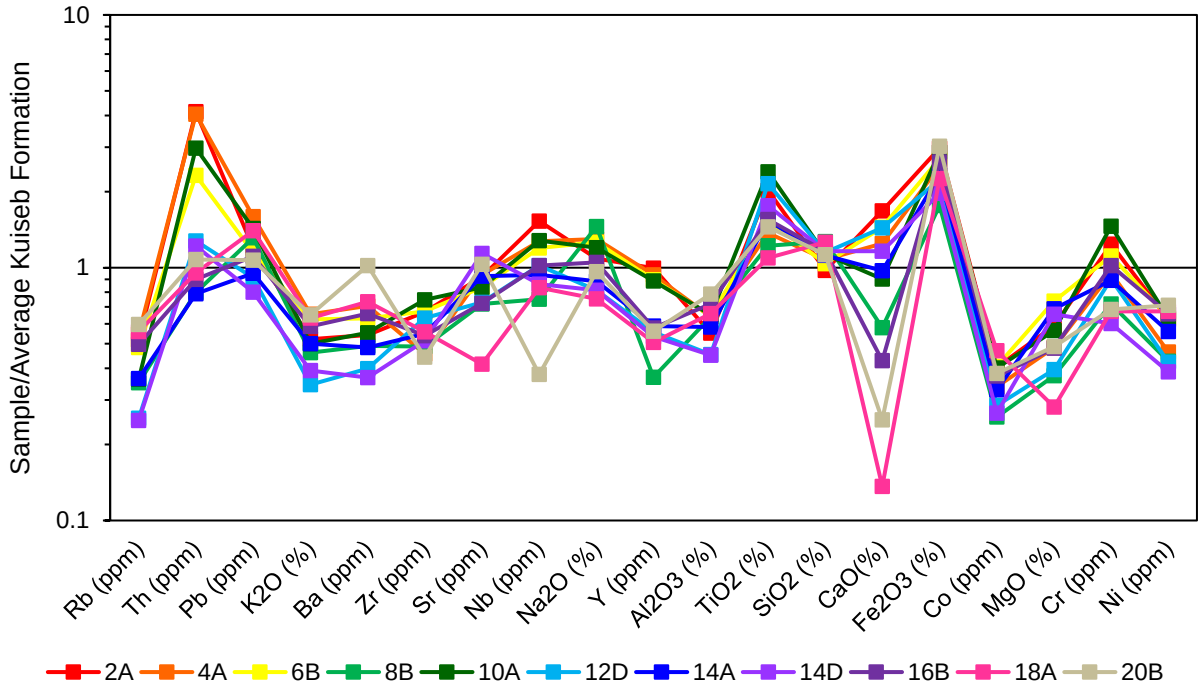

Figure 10. Spider diagram of sample concentration normalized against the Kuiseb Formation with elements arranged in the order of stability.

Chemical Index of Alteration

As the different sample locations move more inland, the CIA gradually increases along the precipitation gradient. Appendix F shows that the CIA ranges from 44% to 72%.

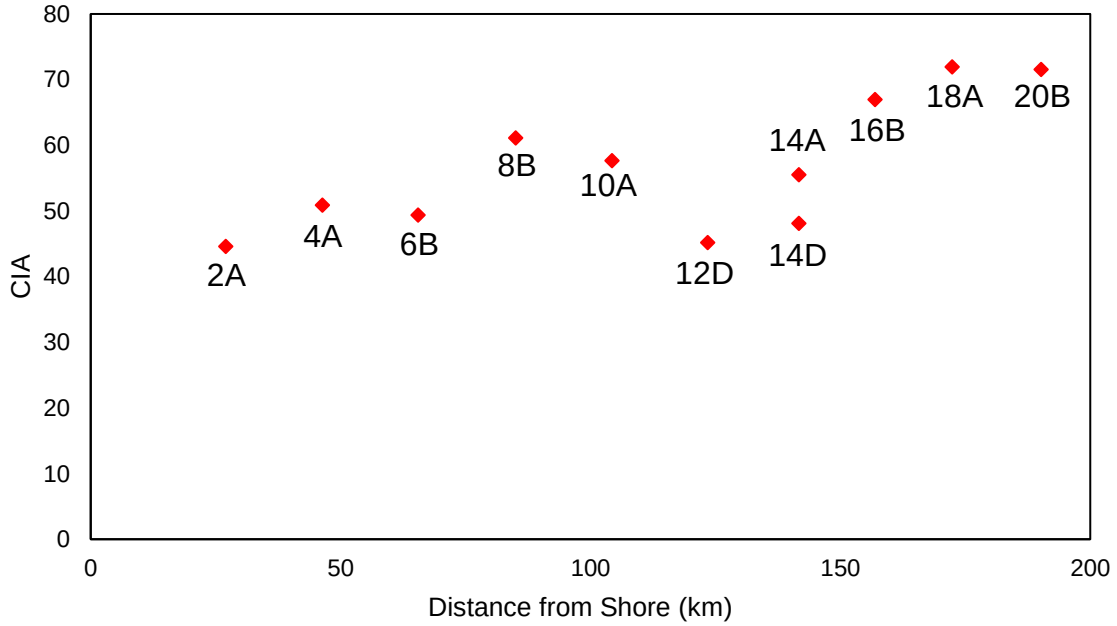

Figure 11. Chemical Index of Alteration (CIA) values in relation to the distance from shore.

DISCUSSION

Elemental Geochemistry of Soil and the Source of Salts in Relation to the Precipitation Gradient

In the locations that are progressively further away from the ocean, more elements typically are depleted. However, the precipitation never exceeds a mean annual value of 250 mm along the entire length of the transect. The gypsum crusts typically occur in areas where there is less than 250 mm of annual precipitation (Watson, 1985).

As one proceeds more inland, the rate of weathering increases as seen in the CIA data (Figure 11). The more intense weathering of the soils occurred from 160 km to 200 km. The last three samples had a CIA greater than 70% as shown in Figure 11 and Appendix F. The CIA values support previous work that demonstrated the mineralogy of the soils progresses from K-Feldspar to illite as the sampling location gets further away from the shore (Bahlburg and Dabrzinski, 2011). The evaporation of groundwater most likely aids the accumulation of salts in the sample sites that are further away from the ocean, since these sample locations are not influenced by the coastal fog, like processes in the Atacama Desert (Rech et. al., 2003). In the Atacama Desert the coastal fog only influenced the first 50 km inland but could not extend further inland because of the elevation differences (Rech, et. al., 2003).

In a comparison of the first sample, 2A, and the last sample, 20B, when normalized against the continental crust, the samples were depleted in Tl, K_2O, Ba, Ta, Hf, Zr, Sr, Na_2O, Al_2O_3, SiO_2, Co, and Ni. Sample 2A was depleted in Cu while the 20B was enriched in the element. Sample 20B was depleted in U, Pb, Ta, Nb, Y, CaO, MgO, and Cr, while the 2A was enriched in these elements and major oxides. There are also some elements in which 2A is more enriched is 20B.

Sample 2A was collected in an area where the coastal fog transports marine aerosols to the land and extends 50 km inland from the coastline (Eckardt et. al., 2012). For example, 2A, is four times more enriched in Th than 20B was. The other elements where the sample 2A seems to be more enriched than 20B occurs in La, Ce, Tb, Lu, and TiO_2. In other arid environments, strontium tends to have a higher level, but Figure 12 is showing that strontium is depleted when compared to the continental crust (Watson, 1985). Sample 2A has an enrichment in CaO more than 20B, which is caused by the coastal fog, which supplies the accumulation of gypsum via marine aerosols.

Further inland, CaO is depleted since the ocean upwelling is not supplying a source of $CaSO_4$ through marine aerosols (Eckardt and Schemenauer, 1998). Figure 12 shows that there is a depletion in CaO which is likely caused by chemical weathering. The CIA values also support the theory of chemical weathering at 20B because Appendix F show the CIA value is 71.6 %. Figure 12 displays the enrichment of the Na_2O and MgO, where 2A has a slightly higher value than 20B, which is more than likely influenced by marine aerosols from the coastal fog, (Eckardt and Schemenauer, 1998).

Figure 12 shows that uranium is enriched relative to the continental crust in 2A, but not in 20B. A possible source of uranium in the desert could be derived from a mineral named carnotite $[K_2(UO_2)_2(VO_4)_2 \bullet 3H_2O]$, which is commonly formed by calcrete, gypcrete, and weathered surfaces (Carlisle, 1983). The carnotite is most likely dissolved into the groundwater which then transports and deposits the uranium at the surface (Carlisle, 1983). A process like this was found

to be occurring in the Western Australia desert, which is another arid environment (Carlisle, 1983).

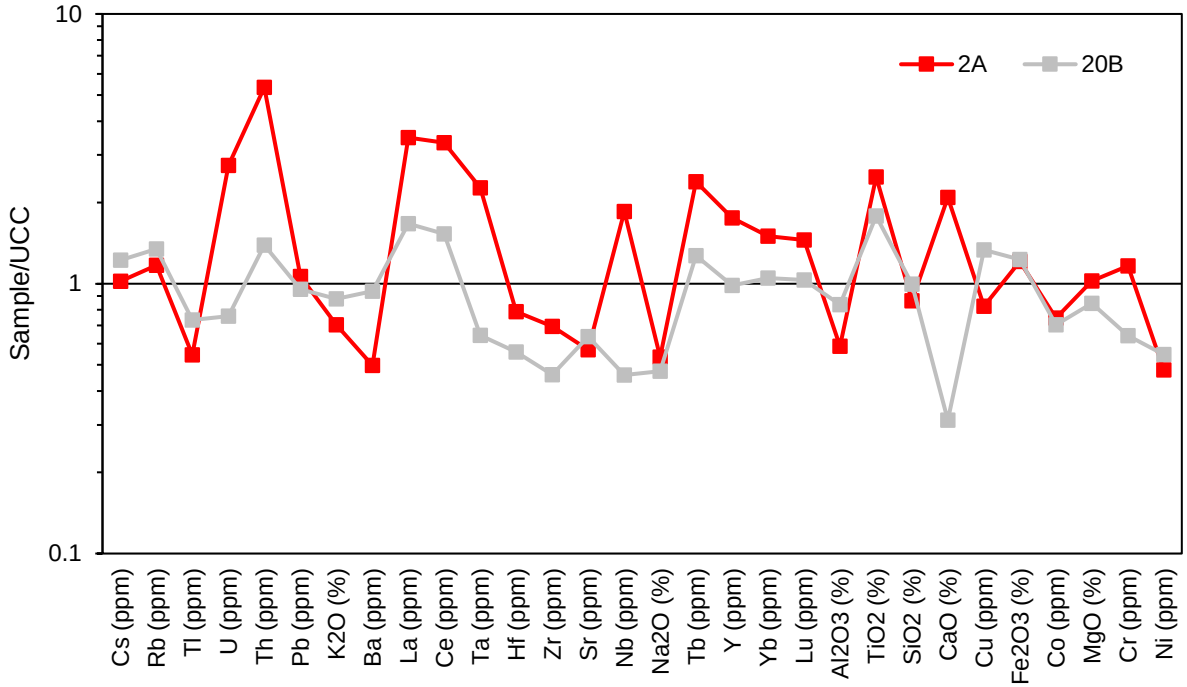

Figure 12. Spider diagram of the first and last sample in the transect compared relative to the Upper Continental Crust.

When 2A and 20B were compared against the Kuiseb Formation, both samples were depleted in Rb, K_2O, Zr, Y, Al_2O_3, Co, MgO, and Ni. The elements 2A was depleted in, while 20B was enriched in, were Ba, Sr, and SiO_2. The elements that 20B was depleted in that 2A was enriched in were Nb, Na_2O, CaO, and Cr. When comparing 2A and 20B the element, Th, 2A is significantly more enriched than 20B. The element, Th, seems to be more enriched in Figure 12 and 13 because it is not as soluble as other elements, leading the element to not be as easily weathered.

Sample 20B is the most weathered, and sample 2A is the least weather due because 2A is from a very arid region. The difference in elemental composition between 2A and 20B is the amount of element lost through chemical weathering or gain through either salt accumulation or relative gain through concentration due to elemental insolubility. The assumption here is that the initial starting materials were the same composition. Figure 14 shows that sample 2A was normalized against sample 20B to determine what elements were lost or gained. In Figure 14, the elements greater than 1 have been lost from the initial soil; these include U, Th, La, Ce, Ta, Hf, Nb, Cr, and especially Ca. The elements at less than 1 are interpreted as having been gained; these include Ba, and perhaps Al and Cu. The other elements fall very close to 1 and therefore it is unclear if there has truly been significant gain or loss. Ca and U are highly mobile elements during soil weathering and have probably been lost over time through chemical weathering. An alternate interpretation is that Ca and U, and perhaps the others mentioned are associated with the gypsum deposits in the most arid part of the desert region (e.g., 2A), and essentially gained

relative to the bulk soils found further inland. As discussed within this text, there are strong arguments for both of these possibilities.

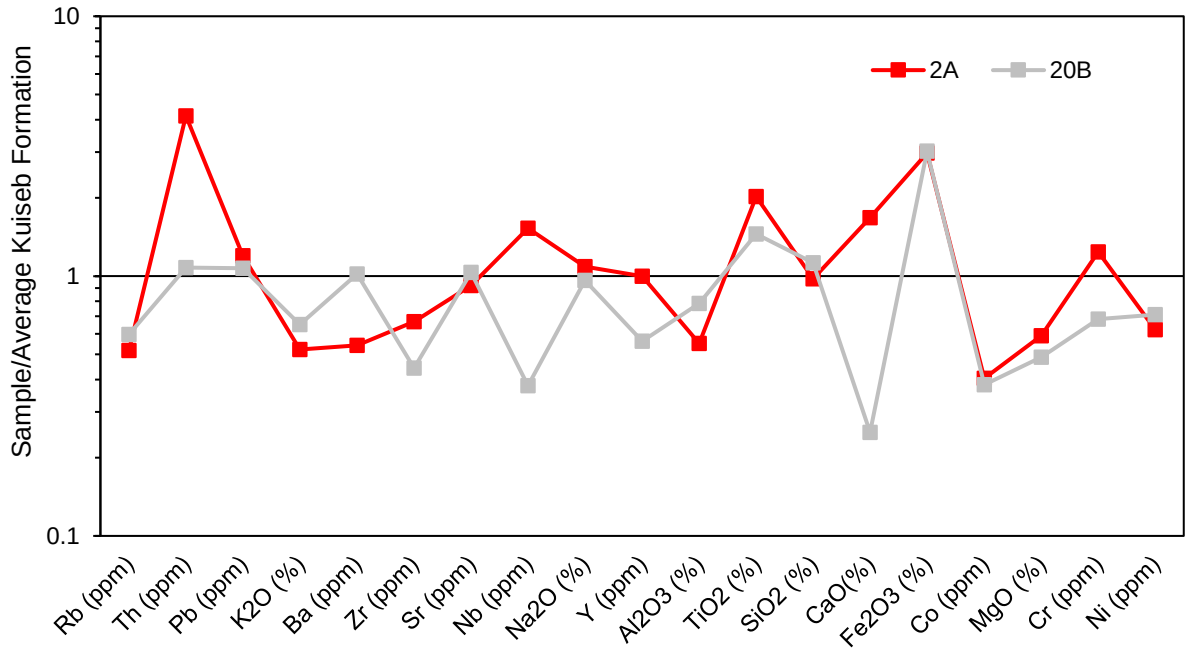

Figure 13. Spider diagram of the first and last sample in the transect compared relative to the Kuiseb Formation.

Figure 14 shows that sample 2A was depleted in Cs, Rb, Tl, K_2O, Ba, Sr, Al_2O_3, SiO_2, Cu, and Ni when compared to sample 20B. Some of the major elements that were enriched were CaO and U. Figure 14 demonstrates that 2A was not as weathered as 20B because most of the elements were enriched compared to 20B. The CIA for 2A had the lowest value of 44.6% indicating that there is little to no weathering occurring in the sample. As the transect progressed in the precipitation gradient, 20B became more weathered indicated by the CIA value of 71.6%.

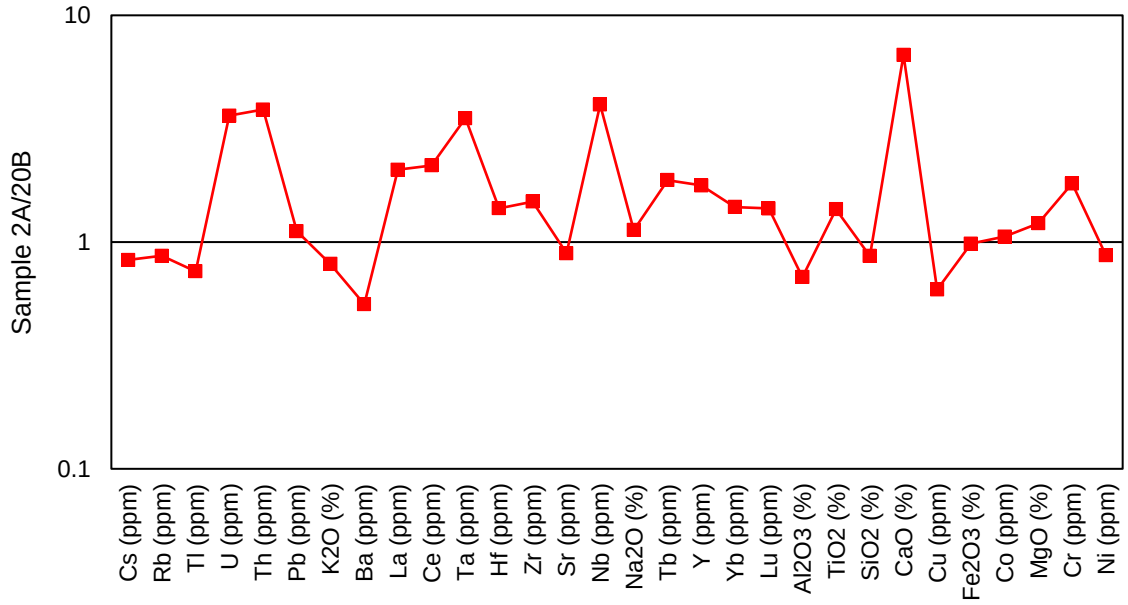

Figure 14. Spider diagram of sample 2A normalized against sample 20B.

Water-Soluble Salt Analysis of the Soil Transect

There is a linear relationship observed between the presence of calcium and bicarbonate (Figure 15). The bicarbonate concentrations were calculated by subtracting the sum of the anions from the sum of the cations. Similarly, when bicarbonate is combined with SO_4 and plotted versus the concentrations of calcium, there is also a linear relationship observed (Figure 16). If the data points fell on the 1:1 in both of these figures it would mean that the primary source of soluble HCO_3 and SO_4 in these soils were either $CaCO_3$ or $CaCO_3$+$CaSO_4$+H_2O. Clearly that is not the case. Other water-soluble salts containing HCO_3 and SO_4 associated with other major cations also exist in theses soils. Their discovery merit further study.

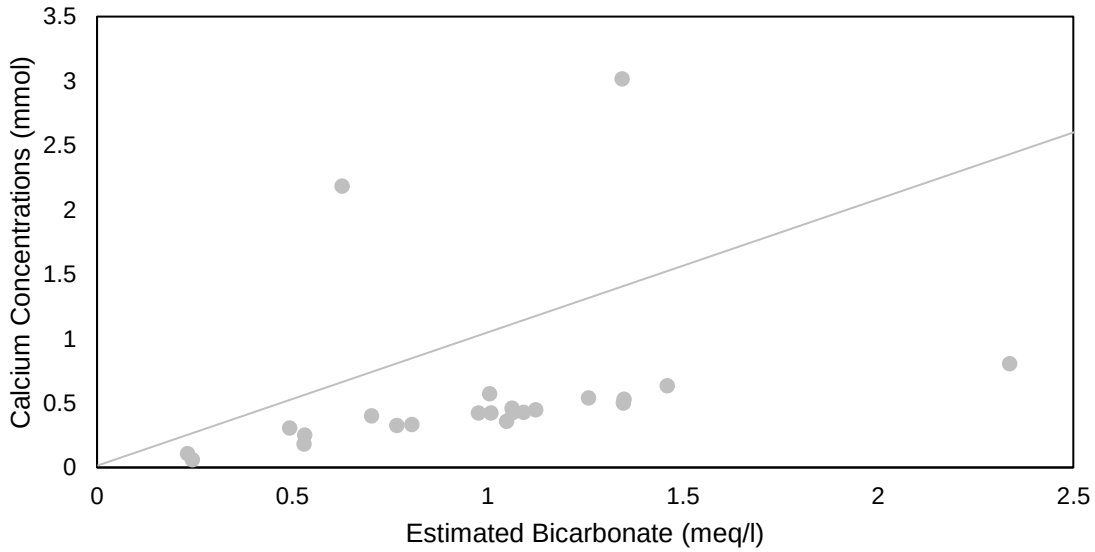

Figure 15. Calcium bicarbonate relationship.

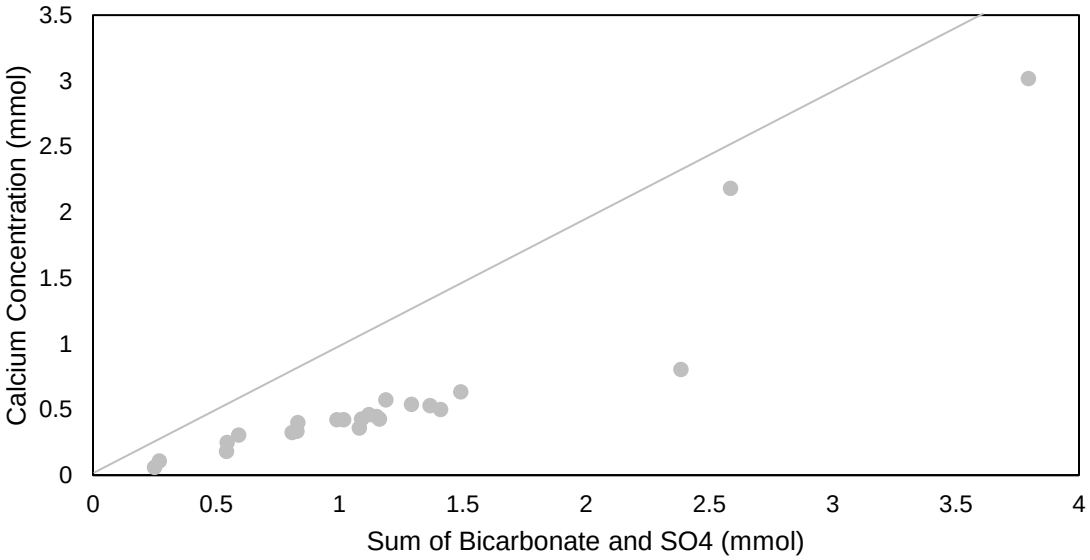

Figure 16. Calcium bicarbonate and SO_4 relationship.

The following figures show the difference in water-soluble salts at nearly the start of the transect, 6A, and the end of the transect, 20D. These two locations were chosen because they represent the climatic extremes in precipitation. Figure 17 shows the nutrient concentrations of the first sample in the transect 6A and the last sample, 20D. 6A and 20D were used to show the difference between the beginning and the end of the transect. The significance of plotting 6A versus 20D was to analyze how water leachable salts are affected by chemical weathering and aridity. 6A had lower concentrations than 20D because most of the nutrients were less than one. 20D was significantly higher in PO_4 and NH_4 than 6A. 6A has a relatively lower concentration in Nitrate and Nitrite than 20B. Sr has the lowest concentration in both soils and appears to mimic the Ca trend. This is not surprising as Sr can substitute for Ca in both aragonite and gypsum. The silica concentration remained relatively the same from the ocean to inland.

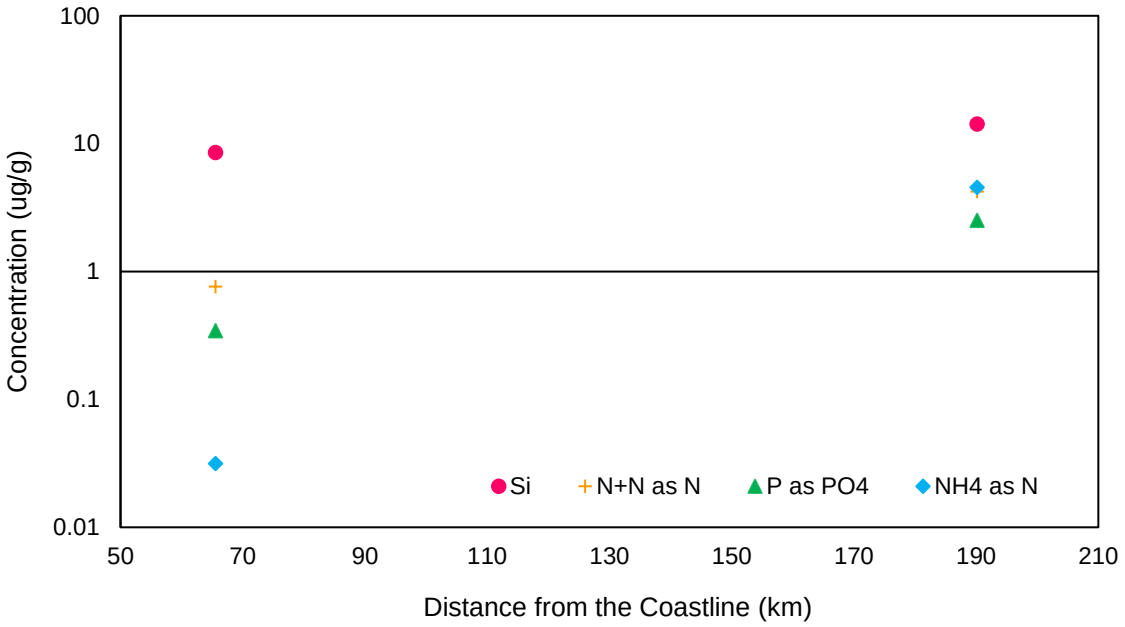

Figure 17. First and last sample location of the nutrient analysis.

Figure 18 showed both samples have concentration of strontium below 1 µg/g. Strontium follows the same pattern in Figure 12 and 13, where strontium is depleted. 6A had a higher concentration of sodium than 20D. 6A had a slightly higher concentration in Ca. 20D was higher in magnesium and potassium. Figure 18 show that from the ocean to inland there is an increase in magnesium and potassium. From the ocean to inland there is a decrease in calcium, sodium, and potassium. Some of the samples had to be filtered more than once because there were a lot of particle <0.4 µm, which may have had an effect on the reading on sample 8D with the measurement of Na on the ICP-OES. The sample was saturated when it was measured with both 10x and 100x dilutions.

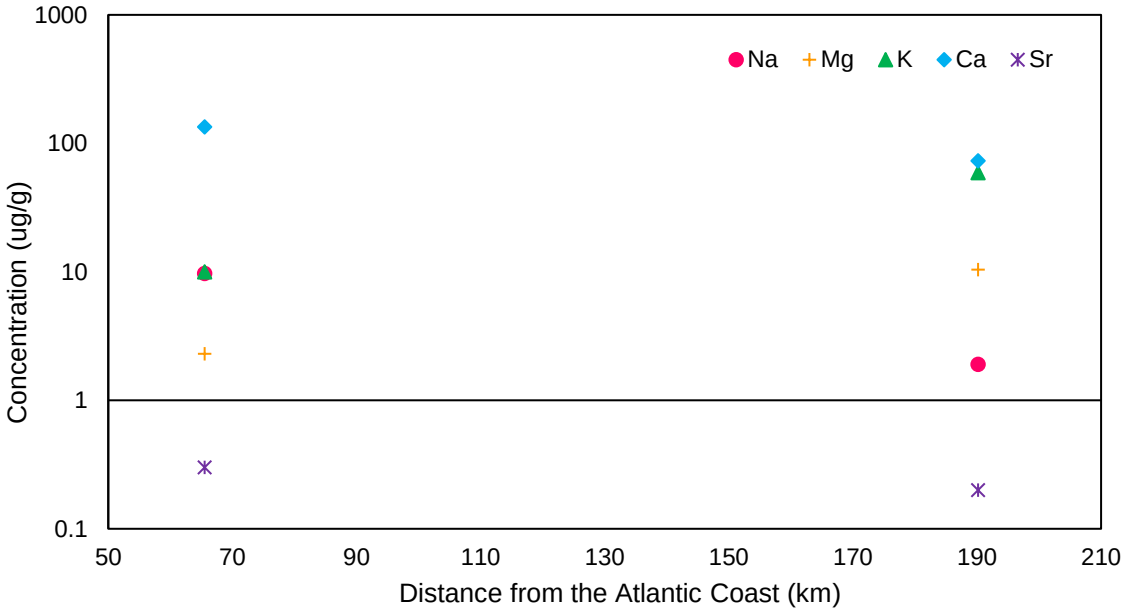

Figure 18. First and last sample locations of cations analysis.

Figure 4 and figure 6 show that both Ca and SO_4 decreases in concentration as the transect progresses. This could indicate that there was a decrease in the concentration of gypsum in the soil as the transect moves farther into the Gravel Plains.

Figure 19 shows 20B had concentrations of NO_3 and PO_4 that never exceeded 1 ppm. 6A's F concentration that never exceeded 1 µg/g. Fluoride was not detected in the samples collected at 200 km inland. 6A had a significantly higher concentration in SO_4 than 20D. From the ocean to inland there is a decrease in SO_4. The concentration of chloride slightly decreases from the ocean to inland. The significant change in concentration for both samples, could be an indicator that 20D is being weathered.

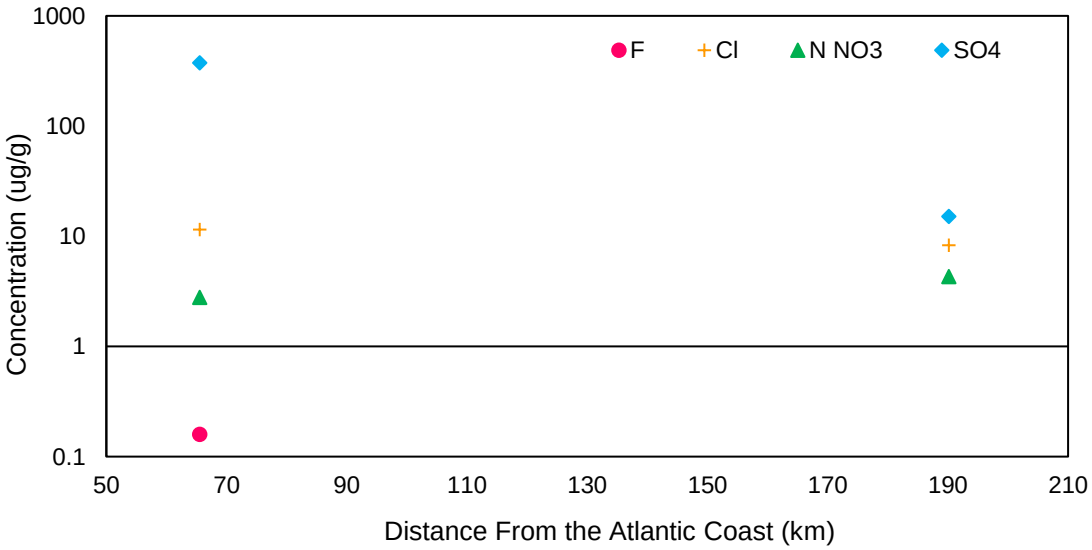

Figure 19. First and last sample location of anions analysis.

Figure 20 shows the values of the water-soluble salts summed up, which was measured from the leachate. The highest sum of the salts occurred at 80 km. There was a sharp drop in the sum of the salts around 100 km from the Atlantic Ocean. The lowest sum of the leachable salts happened around 170 km. Generally, the sum of the sample concentration decreased as the transect progressed inland.

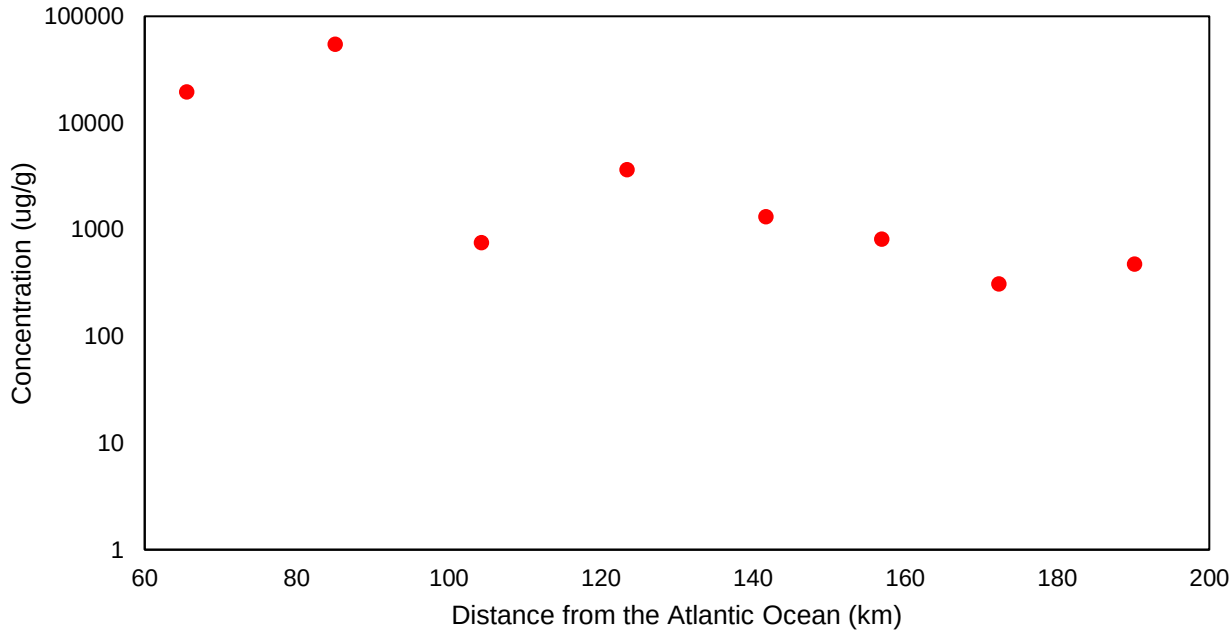

Figure 20. Sum of all the leachable salts in μg/g in relation to the Atlantic Coast.

CONCLUSIONS

The objectives of this study were to determine the geochemistry of the Central Namib Desert soils and to understand how the soils change with distance from the coastline along a precipitation and climate gradient.

In order to determine the soluble geochemistry, soil samples were leached with water and chemical analysis was used to measure the cations, anions, and nutrients. In addition, to understand if the soils were chemically weathered, solid samples were analyzed by XRF and CIAs were calculated. This allowed for analysis of the total elemental concentrations in the soil to be compared to the UCC values. The XRF analysis proves that as the soils progressively inland, the soils are more chemically weathered. The research achieved the primary objectives by analyzing the changes in geochemistry of the soil and how it changes with the process of weathering and the precipitation gradient in the desert.

The datum show that there is more accumulation of salt occurring closer to the coastline and the samples collected further away from the coast demonstrate affects of chemical weathering. The samples collected closer to the coastline are mostly influenced by the ocean upwelling; resulting marine aerosols to be transported inland and then be deposited in the soil. The soils closer to the ocean were enriched in CaO, whereas the sample farthest from the ocean was depleted. Ca is one of the elements used to form gypsum. There were also higher concentrations of SO_4 in soils closer to the coast, suggesting that marine aerosols are a major source of the accumulation of salts. Sample 2A has a CIA of 44.6%, while 20B has a value of 71.6% indicating more chemical weathering of the soils has occurred at this latter location. Annual mean precipitation increases from <50 mm to 200-250 mm from 2A to 20B eastward along the transect. The research strongly supports that climate influences the rates of chemical weathering through precipitation. This work also suggests that coastal fog plays an important role in salt deposition in the most arid portions of the region.

RECOMMENDATIONS FOR FUTURE WORK

The way that the soil is collected could be done differently. Instead of collecting surficial soils different depths could be collected in order to analyze how moisture changes with depth with a distance from the shore. Isotopic analysis could be completed to determine the difference between chemical weathering and fog influences to distinguish the major source of deposition. Stable isotope analysis for C, S, and N of the water-soluble salts would greatly aid in the determination of their sources. Salt concentrations with depth in soil profiles could be evaluated in order to examine the role of both surface water recharge, and groundwater wicking in accumulation of salts. The SEM can determine the mineralogy of the soils, and more importantly the pedogenesis of gypsum. The SEM can be used to determine if there is weathering of exposed bedrock that is occurring, which contributes to the accumulation of salts in the soil. X-ray diffraction analyses along with SEM work would aid in determining what the primary minerals are present being weathered.

REFERENCES CITED

Atlas of Namibia Project, (2003) Directorate of Environmental Affairs, Ministry of Environment and Tourism. http://www.dea.met.gov.na

Bahlburg H. and Dobrzinski N. (2011) A review of the Chemical Index of Alteration (CIA) and its application to the study of Neoproterozoic glacial deposits and climate transitions. *Geological Society, London, Memoirs*. vol. 36, pp. 81-92. doi:10.1144/M36.6

Carlisle D. (1983) Concentration of uranium and vanadium in calcretes and gypcretes. *Geological Society, London, Special Publications.* vol. 11, pp. 185-195. doi: 10.1144/GSL.SP.1983.011.01.19

Dombrowski, A., Hoernes, S., and Okrusch, M. (1996) Scapolitization in the Kuiseb Formation of the Damara Orogen: geochemical and sTable Isotope evidence for fluid infiltration along deep crustal shear zone. *Communications Geological Survey, Namibia*. vol. 11, pp. 23-31.

Eckardt F. D. and Schemenauer R. S. (1998) Fog Water Chemistry in the Namib Desert, Namibia. *Atmospheric Environment*. vol. 32, no. 14/15, pp. 2595-2599. doi: 10.1016/S1352-2310(97)00498-6

Eckardt F. D., Soderberg K., Coop L. J., Muller A. A., Vickery K. J., Grandin R. D., Jack C., Kapalanga T. S., Henschel J. (2012) The nature of moisture at Gobabeb, in the central Namib Desert. *Journal of Arid Environments*. pp. 1-13. doi:10.1016/j.jaridenv.2012.01.011

Frick, S.E. & Hijmans, R. J. (2017) Worldclim 2: New 1 km spatial resolution climate surfaces for global land areas. *International Journal of Climatology.*

Nesbitt, H.W., and Young, G.M. (1982) Early Proterozoic climates and plate motions inferred from major element chemistry of lutites: Nature, v. 299, p. 715–717. doi:10.1038/299715a0

Prave, A. R. (1996) Tale of Three Cratons: Tectonostratigraphic anatomy of the Damara orogen in northwestern Namibia and the assembly of Gondwana. *Geology*. vol. 24, no. 12, p. 1115-1118.

Rech J. A., Quade J., and Hart W. S. (2003) Isotopic evidence for the source of Ca and S in soil gypsum, anhydrite and calcite in the Atacama Desert, Chile. *Geochimica et Cosmochimica Acta*. vol. 67, no. 4, pp. 575-586. doi:10.1016/S0016-7037(02)01175-4

Viles, H. and Goudie, A., 2013, Weathering in the central Namib Desert, Namibia: Controls, processes and implications: Journal of Arid Environments, v. 93, p. 20-29, doi: 10.1016/j.jaridenv.2011.09.012.

Watson A. (1985) Structure, chemistry and origins of gypsum crusts in southern Tunisia and the central Namib Desert. *Sedimentology*. 32, 855-875. doi:10.1111/j.1365-3091.1985.tb00737.x

APPENDICES

Appendix A. Sample Information and Location

Site Name	GPS Coordinates	Elevation (m)
C14-2-A	S22˚59.979' E014˚40.294'	115
C14-2-B	S23˚00.012' E014˚40.292'	115
C14-2-C	S23˚00.111' E014˚40.284'	114
C14-2-D	S23˚00.144' E014˚40.289'	113
C14-4-A	S23˚01.016' E014˚51.547'	314
C14-4-B	S23˚01.040' E014˚51.566'	316
C14-4-C	S23˚01.127' E014˚51.585'	322
C14-4-D	S23˚01.169' E014˚51.567'	316
C14-6-A	S23˚03.900' E015˚02.417'	529
C14-6-B	S23˚03.943' E015˚02.401'	528
C14-6-C	S23˚04.032' E015˚02.387'	527
C14-6-D	S23˚04.055' E015˚02.395'	528
C14-8-A	S23˚08.554' E015˚12.578'	617
C14-8-B	S23˚08.564' E015˚12.552'	616
C14-8-C	S23˚08.603' E015˚12.466'	615
C14-8-D	S23˚08.620' E015˚12.414'	613
C14-10-A	S23˚14.714' E015˚21.663'	756
C14-10-B	S23˚14.754' E015˚21.648'	753
C14-10-C	S23˚14.819' E015˚21.609'	750
C14-10-D	S23˚14.852' E015˚21.599'	751
C14-12-A	S23˚18.585' E015˚32.033'	943
C14-12-B	S23˚18.622' E015˚32.027'	942
C14-12-C	S23˚18.694' E015˚32.023'	938
C14-12-D	S23˚18.738' E015˚32.003'	938
C14-14-A	S23˚19.441' E015˚42.843'	886
C14-14-B	S23˚19.467' E015˚42.860'	888
C14-14-C	S23˚19.558' E015˚42.868'	889
C14-14-D	S23˚19.582' E015˚42.855'	889
C14-16-A	S23˚19.222' E015˚51.809'	962
C14-16-B	S23˚19.213' E015˚51.777'	963
C14-16-C	S23˚19.194' E015˚51.701'	954
C14-16-D	S23˚19.184' E015˚51.668'	968
C14-18-A	S23˚20.678' E016˚00.587'	1084
C14-18-B	S23˚20.685' E016˚00.611'	1085
C14-18-C	S23˚20.346' E016˚00.684'	1082
C14-18-D	S23˚20.769' E016˚00.689'	1082
C14-20-A	S23˚14.686' E016˚08.574'	1255
C14-20-B	S23˚14.699' E016˚08.595'	1255
C14-20-C	S23˚14.759' E016˚08.666'	1248
C14-20-D	S23˚14.773' E016˚08.684'	1249

Appendix B. IC Concentrations in μg/g.

Site Name	Dilution Factor	F	Cl	Br	N as NO3	SO4
C14-6-A	25x	0.16	11.5		2.8	376.6
C14-6-B	25x	0.4	1727		42.8	3558
C14-6-C	25x	0.1	9		0.45	5915
C14-6-D	25x	0.09	12		0.45	2333
C14-8-A	25x	0.34	9485		7.9	2093
C14-8-B			5.4			24.7
C14-8-C	25x	0.99	16825	11.7	1513	7565
C14-8-D	25x	0.22	6.5		8.55	2055
C14-10-A		0.1	9.55	0.6		33.4
C14-10-B		0.05	2.05			12
C14-10-C		0.3	54.5	0.15	2.55	61.7
C14-10-D		0.3	1.85			27.2
C14-12-A		0.25	0.55		0.05	15.4
C14-12-B		0.2	3.05			16.3
C14-12-C	25x	0.87	14.5	21.8	1.45	940.5
C14-12-D	25x	1.74	17		2.2	1177
C14-14-A			221	0.95		102.6
C14-14-B			165	0.75	0.5	87.7
C14-14-C		0.05	14.9		1.1	19.4
C14-14-D		0.1	72.9	0.35	0.75	46.7
C14-16-A		0.75	11		6.1	12.8
C14-16-B		0.2	13.9		0.45	30.1
C14-16-C		0.1	2.75			8.7
C14-16-D	2x	0.1	5.9		1.4	23.3
C14-18-A		0.2	3.5			18.3
C14-18-B		0.05	1.35			2.35
C14-18-C			1.95		8.75	6.25
C14-18-D			3.3	0.1	2.8	6.25
C14-20-A			1.5		0.05	4.1
C14-20-B		0.15	2.65		1.2	5.65
C14-20-C		0.05	2.1			10.3
C14-20-D	2x		8.3		4.3	15.2

*Blank cells were due the machine not being able to detect the values.

Appendix C. Nutrient Analyzer Concentrations in μg/g.

Site Name	Si	N+N as N	P as PO4	NH4 as N
C14-6-A	8.507	0.762	0.344	0.032
C14-6-B	23.54	37.89	0.009	0.014
C14-6-C	9.433	0.307	0.477	0.009
C14-6-D	4.331	0.261	0.053	-0.009
C14-8-A	13.15	5.623	0.019	0.021
C14-8-B	7.881	0.414	0.261	0.026
C14-8-C	12.20	0.014	0.035	-0.013
C14-8-D	16.03	1490	0.021	0.251
C14-10-A	16.60	0.773	0.889	0.079
C14-10-B	16.26	0.668	0.762	0.089
C14-10-C	15.45	2.251	0.722	0.204
C14-10-D	13.66	0.112	0.253	0.029
C14-12-A	18.09	0.073	0.714	0.124
C14-12-B	18.24	0.073	0.714	0.124
C14-12-C	16.07	1.827	0.141	0.008
C14-12-D	15.91	1.153	0.141	0.008
C14-14-A	13.6	0.047	0.775	1.356
C14-14-B	11.00	0.417	0.407	1.356
C14-14-C	12.04	0.899	1.256	1.422
C14-14-D	10.04	0.598	0.493	0.494
C14-16-A	10.97	4.822	0.253	0.392
C14-16-B	5.936	0.198	0.646	1.212
C14-16-C	11.46	0.745	0.608	0.058
C14-16-D	16.07	1.262	1.877	5.728
C14-18-A	11.51	0.122	2.842	0.084
C14-18-B	8.675	0.065	2.367	0.045
C14-18-C	11.47	8.988	2.138	0.644
C14-18-D	11.02	3.866	5.107	0.518
C14-20-A	14.08	0.007	0.943	0.021
C14-20-B	13.91	1.703	1.644	1.124
C14-20-C	14.87	0.592	1.174	0.466
C14-20-D	14.27	4.226	2.51	4.565

Appendix D. ICP-OES Concentrations in μg/g.

Site Name	Dilution Factor	Li	Na	Mg	K	Ca	Sr	Ba
C14-6-A	2x	<0.1	9.70	2.3	10	134	0.3	<0.1
C14-6-B	10x	<0.1	1137	32	145	1130	3	<0.1
C14-6-C	10x	<0.1	24.00	8.5	24.65	2130	3.75	<0.1
C14-6-D	10x	<0.1	12.10	3.3	7.95	689	1.55	<0.1
C14-8-A	100x	<0.1	8315	15	50	850	5	<0.1
C14-8-B	2x	<0.1	9.50	1.3	6	51	0.2	<0.1
C14-8-C	10x	<0.1	11.60	4.75	14.6	675	1.85	<0.1
C14-8-D	100x	<0.1		25	1550	3300	25	<0.1
C14-10-A	2x	<0.1	21.00	5.3	31	87	0.4	<0.1
C14-10-B	2x	<0.1	10.60	4.4	20	87	0.3	<0.1
C14-10-C	10x	<0.1	24.75	5.25	36.4	81.5	0.4	<0.1
C14-10-D	10x	<0.1	10.95	3.65	19.15	93.8	0.4	<0.1
C14-12-A	2x	<0.1	4.60	5.1	23	129	0.4	<0.1
C14-12-B	2x	<0.1	6.00	4.7	23	110	0.4	<0.1
C14-12-C	10x	<0.1	6.50	6.5	20	445	2.5	<0.1
C14-12-D	10x	<0.1	4.50	6.5	15	615	4	<0.1
C14-14-A	10x	<0.1	30.60	5.2	26.7	41.85	0.35	<0.1
C14-14-B	10x	<0.1	63.75	16.45	61.6	116.65	1.05	<0.1
C14-14-C	10x	<0.1	7.90	7.85	16.35	66.25	0.65	<0.1
C14-14-D	10x	<0.1	20.45	8.45	33.05	62.2	0.6	<0.1
C14-16-A	2x	<0.1	8.9	13.7	20	91	0.5	<0.1
C14-16-B	2x	<0.1	19	12.3	33	102	0.4	<0.1
C14-16-C	2x	<0.1	2.9	14.1	15	108	0.3	<0.1
C14-16-D	2x	<0.1	3.1	35.1	47	164	1	<0.1
C14-18-A	2x	<0.1	3.2	4.1	3.1	22	0.1	<0.1
C14-18-B	2x	<0.1	1.9	2.7	16	12	0.1	<0.1
C14-18-C	2x	<0.1	1.3	4.5	20	51	0.1	<0.1
C14-18-D	2x	<0.1	1.8	7.9	14	86	0.2	<0.1
C14-20-A	2x	<0.1	1.3	4.4	18	86	0.1	<0.1
C14-20-B	2x	<0.1	2.1	5.4	23	37	0.1	<0.1
C14-20-C	2x	<0.1	1.7	4.8	19	68	0.1	<0.1
C14-20-D	2x	<0.1	1.9	10.4	59	73	0.2	<0.1

Appendix E1. XRF Concentrations (trace elements)

Elements	2A	4A	6B	8B	10A	12D	14A	14D	16B	18A	20B
Ag (ppm)	0.06	0.03	0.06	0.02	0.07	0.03	0.03	0.03	0.04	0.11	0.1
Ba (ppm)	311	406	362	282	318	229	278	211	378	421	585
Cr (ppm)	107	82	96	62	126	78	77	52	88	58	59
Cu (ppm)	23.1	15.7	22.4	12.6	16.1	12.1	17.9	14.1	17.5	24.3	37.4
Li (ppm)	27	19	26	21	21	13	21	15	26	23	27
Mn (ppm)	848	687	748	611	860	647	776	667	713	783	562
Ni (ppm)	22.5	16.8	23	15.4	22.8	15.3	20.2	14	23.7	24.3	25.7
P (ppm)	970	1028	1162	670	994	404	685	305	312	603	670
Sr (ppm)	182	185	165	142	165	144	183	225	143	82	204
V (ppm)	133	98	121	72	132	131	97	81	94	66	72
Zn (ppm)	50	42	54	37	49	31	50	35	53	45	60
Zr (ppm)	134	91.5	135	98	150	127	110	103	108	112	88.9
As (ppm)	3	3	7	6	3	5	8	7	4	3	2
Be (ppm)	1.5	2.5	1.8	2.1	2.1	1.6	1.8	1.3	1.8	2.1	2.8
Bi (ppm)	0.2	0.15	0.31	0.22	0.24	0.17	0.2	0.16	0.24	0.25	0.26
Cd (ppm)	0.14	0.12	0.2	0.12	0.18	0.13	0.12	0.1	0.13	0.12	0.13
Ce (ppm)	210	181	158	62.5	204	75.36	62.09	57.98	72.53	83.25	96.44
Co (ppm)	12.9	10.8	13	8.2	12.8	9.1	10.5	8.5	11.9	15	12.2
Cs (ppm)	5	3	4	4	3	2	3	2	4	4	6
Ga (ppm)	11.2	12.8	12.8	10.3	11.7	8	10.9	7.7	14.1	12.7	15.1
Hf (ppm)	4.17	2.91	4.08	3.11	4.98	4.07	3.37	3.04	3.38	3.43	2.96
Ln (ppm)	0.05	0.04	0.06	0.03	0.05	0.04	0.05	0.03	0.07	0.05	0.05
La (ppm)	108	94.2	80.4	32.3	106	38.5	31.4	29.8	37.4	43	51.8
Lu (ppm)	0.45	0.36	0.39	0.22	0.43	0.36	0.36	0.33	0.34	0.28	0.32
Mo (ppm)	0.71	0.84	0.94	0.56	0.58	0.6	0.68	0.45	0.51	0.72	1.79
Nb (ppm)	22.2	18.5	17.4	10.9	18.6	14.8	13.6	12.5	14.8	12.1	5.5
Pb (ppm)	18.1	24.1	17.4	19.9	21.6	13.8	14.4	12.1	16.8	21.2	16.2
Rb (ppm)	98.2	104	91.8	66.6	68.7	48.1	69.1	47.2	94.5	106	113
Sb (ppm)	0.14	0.12	0.17	0.08	0.15	0.13	0.12	0.09	0.17	0.12	0.05
Sc (ppm)	14.3	11.7	14.3	8.6	14.4	10.2	11.4	8.2	13.7	10	11.8
Se (ppm)	2	2	2	2	2	2	2	2	2	2	2
Sn (ppm)	4.5	2.5	2.9	2	2.4	1.6	2.3	1.6	2.5	2.3	2.2
Ta (ppm)	2.04	1.59	1.45	1.07	2.14	1.28	1.24	1.18	1.35	1.14	0.58
Tb (ppm)	1.67	1.58	1.41	0.6	1.67	0.74	0.73	0.64	0.81	0.8	0.89
Te (ppm)	0.05	0.05	0.05	0.05	0.05	0.05	0.05	0.05	0.05	0.05	0.05
Th (ppm)	56.1	54.9	31.4	10.8	40.3	17.3	10.7	16.5	12.2	12.9	14.6
Tl (ppm)	0.49	0.57	0.51	0.41	0.39	0.27	0.37	0.27	0.55	0.58	0.66
U (ppm)	7.4	6.21	5.79	3.24	7.13	3.75	2.56	3.22	2.25	2.38	2.05
W (ppm)	1	0.9	1.2	1	1.1	1.1	1.1	1	1.2	1.1	1.3
Y (ppm)	36.8	34.6	33.1	13.6	32.7	20.5	21.7	19.7	21.3	18.7	20.7
Yb (ppm)	3	2.5	2.7	1.4	2.8	2.3	2.3	2.3	2.3	1.9	2.1

Appendix E2. XRF Concentrations (major and minor elements)

Elements	2A	4A	6B	8B	10A	12D	14A	14D	16B	18A	20B
SiO_2 (%)	57.6	63.5	61.1	74.8	66.5	67.8	66	68.5	68.4	74.3	66.3
Al_2O_3 (%)	9.04	10.5	10.6	10.5	10.7	7.45	9.56	7.41	11.8	10.8	12.9
Fe_2O_3 (%)	6.09	5.17	5.53	3.61	5.87	4.56	4.76	4.04	5.37	4.61	6.19
MgO (%)	2.54	2.08	3.18	1.61	2.43	1.7	2.96	2.82	2.07	1.21	2.1
CaO (%)	7.5	5.57	6.47	2.59	4.03	6.43	4.35	5.2	1.92	0.61	1.12
K_2O (%)	1.97	2.47	2.36	1.74	1.89	1.3	1.89	1.48	2.21	2.39	2.46
Na_2O (%)	1.75	2.09	2.03	2.34	1.93	1.31	1.42	1.31	1.69	1.21	1.55
TiO_2 (%)	1.59	1.08	1.21	0.96	1.88	1.69	1.21	1.38	1.22	0.86	1.14
MnO (%)	0.12	0.09	0.11	0.08	0.13	0.1	0.11	0.11	0.1	0.1	0.08
P_2O_5 (%)	0.22	0.23	0.3	0.17	0.25	0.1	0.18	0.09	0.08	0.15	0.16
Cr_2O_3 (%)	0.02	0.02	0.03	0.01	0.03	0.02	0.02	0.01	0.01	0.01	0.01
V_2O_5 (%)	0.02	0.02	0.02	0.01	0.03	0.03	0.02	0.01	0.02	0.01	0.01

Appendix F. Chemical Index Alteration

Sample	Al_2O_3	CaO	Na_2O	K_2O	CIA
2A	9.04	7.5	1.75	1.97	44.6
4A	10.5	5.57	2.09	2.47	50.9
6B	10.6	6.47	2.03	2.36	49.4
8B	10.5	2.59	2.34	1.74	61.2
10A	10.7	4.03	1.93	1.89	57.7
12D	7.45	6.43	1.31	1.3	45.2
14A	9.56	4.35	1.42	1.89	55.5
14D	7.41	5.2	1.31	1.48	48.1
16B	11.8	1.92	1.69	2.21	67
18A	10.8	0.61	1.21	2.39	72
20B	12.9	1.12	1.55	2.46	71.6

Appendix G. XRF Values Normalized Against Continental Crust

Elements	2A	4A	6B	8B	10A	12D	14A	14D	16B	18A	20B
Cs (ppm)	1.02	0.61	0.82	0.82	0.61	0.41	0.61	0.41	0.82	0.82	1.22
Rb (ppm)	1.17	1.24	1.09	0.79	0.82	0.57	0.82	0.56	1.13	1.26	1.35
Tl (ppm)	0.54	0.63	0.57	0.46	0.43	0.30	0.41	0.30	0.61	0.64	0.73
U (ppm)	2.74	2.30	2.14	1.20	2.64	1.39	0.95	1.19	0.83	0.88	0.76
Th (ppm)	5.34	5.23	2.99	1.03	3.84	1.65	1.02	1.57	1.16	1.23	1.39
Pb (ppm)	1.06	1.42	1.02	1.17	1.27	0.81	0.85	0.71	0.99	1.25	0.95
K2O (%)	0.70	0.88	0.84	0.62	0.68	0.46	0.68	0.53	0.79	0.85	0.88
Ba (ppm)	0.50	0.65	0.58	0.45	0.51	0.37	0.45	0.34	0.61	0.67	0.94
La (ppm)	3.48	3.04	2.59	1.04	3.42	1.24	1.01	0.96	1.21	1.39	1.67
Ce (ppm)	3.33	2.87	2.51	0.99	3.24	1.20	0.99	0.92	1.15	1.32	1.53
Ta (ppm)	2.27	1.77	1.61	1.19	2.38	1.42	1.38	1.31	1.50	1.27	0.64
Hf (ppm)	0.79	0.55	0.77	0.59	0.94	0.77	0.64	0.57	0.64	0.65	0.56
Zr (ppm)	0.69	0.47	0.70	0.51	0.78	0.66	0.57	0.53	0.56	0.58	0.46
Sr (ppm)	0.57	0.58	0.52	0.44	0.52	0.45	0.57	0.70	0.45	0.26	0.64
Nb (ppm)	1.85	1.54	1.45	0.91	1.55	1.23	1.13	1.04	1.23	1.01	0.46
Na2O (%)	0.54	0.64	0.62	0.72	0.59	0.40	0.43	0.40	0.52	0.37	0.47
Tb (ppm)	2.39	2.26	2.01	0.86	2.39	1.06	1.04	0.91	1.16	1.14	1.27
Y (ppm)	1.75	1.65	1.58	0.65	1.56	0.98	1.03	0.94	1.01	0.89	0.99
Yb (ppm)	1.50	1.25	1.35	0.70	1.40	1.15	1.15	1.15	1.15	0.95	1.05
Lu (ppm)	1.45	1.16	1.26	0.71	1.39	1.16	1.16	1.06	1.10	0.90	1.03
Al2O3 (%)	0.59	0.68	0.69	0.68	0.69	0.48	0.62	0.48	0.77	0.70	0.84
TiO2 (%)	2.48	1.69	1.89	1.50	2.94	2.64	1.89	2.16	1.91	1.34	1.78
SiO2 (%)	0.86	0.95	0.92	1.12	1.00	1.02	0.99	1.03	1.03	1.12	1.00
CaO (%)	2.09	1.55	1.80	0.72	1.12	1.79	1.21	1.45	0.53	0.17	0.31
Cu (ppm)	0.83	0.56	0.80	0.45	0.58	0.43	0.64	0.50	0.63	0.87	1.34
Fe2O3 (%)	1.21	1.03	1.10	0.72	1.16	0.90	0.94	0.80	1.07	0.91	1.23
Co (ppm)	0.75	0.62	0.75	0.47	0.74	0.53	0.61	0.49	0.69	0.87	0.71
MgO (%)	1.02	0.84	1.28	0.65	0.98	0.69	1.19	1.14	0.83	0.49	0.85
Cr (ppm)	1.16	0.89	1.04	0.67	1.37	0.85	0.84	0.57	0.96	0.63	0.64
Ni (ppm)	0.48	0.36	0.49	0.33	0.49	0.33	0.43	0.30	0.50	0.52	0.55

Appendix H. XRF Concentrations Normalized Against Kuiseb Formation

Elements	2A	4A	6B	8B	10A	12D	14A	14D	16B	18A	20B
Rb (ppm)	0.52	0.55	0.48	0.35	0.36	0.25	0.36	0.25	0.50	0.56	0.60
Th (ppm)	4.14	4.05	2.32	0.80	2.97	1.28	0.79	1.22	0.90	0.95	1.08
Pb (ppm)	1.20	1.59	1.15	1.32	1.43	0.91	0.95	0.80	1.11	1.40	1.07
K_2O (%)	0.52	0.65	0.63	0.46	0.50	0.34	0.50	0.39	0.59	0.63	0.65
Ba (ppm)	0.54	0.71	0.63	0.49	0.55	0.40	0.48	0.37	0.66	0.73	1.02
Zr (ppm)	0.67	0.46	0.67	0.49	0.75	0.63	0.55	0.51	0.54	0.56	0.44
Sr (ppm)	0.92	0.94	0.84	0.72	0.84	0.73	0.93	1.14	0.72	0.41	1.03
Nb (ppm)	1.53	1.27	1.20	0.75	1.28	1.02	0.94	0.86	1.02	0.83	0.38
Na_2O (%)	1.09	1.30	1.26	1.45	1.20	0.81	0.88	0.81	1.05	0.75	0.96
Y (ppm)	1.00	0.94	0.90	0.37	0.89	0.56	0.59	0.53	0.58	0.51	0.56
Al_2O_3 (%)	0.55	0.64	0.65	0.64	0.65	0.45	0.58	0.45	0.72	0.66	0.79
TiO_2 (%)	2.02	1.37	1.54	1.22	2.39	2.15	1.54	1.76	1.55	1.09	1.45
SiO_2 (%)	0.98	1.08	1.04	1.27	1.13	1.15	1.12	1.16	1.16	1.26	1.12
CaO(%)	1.68	1.25	1.45	0.58	0.90	1.44	0.97	1.16	0.43	0.14	0.25
Fe_2O_3 (%)	2.97	2.52	2.70	1.76	2.87	2.23	2.32	1.97	2.62	2.25	3.02
Co (ppm)	0.40	0.34	0.41	0.26	0.40	0.28	0.33	0.27	0.37	0.47	0.38
MgO (%)	0.59	0.48	0.74	0.37	0.56	0.39	0.69	0.65	0.48	0.28	0.49
Cr (ppm)	1.24	0.95	1.11	0.72	1.46	0.90	0.89	0.60	1.02	0.67	0.68
Ni (ppm)	0.62	0.46	0.64	0.43	0.63	0.42	0.56	0.39	0.66	0.67	0.71

Appendix I. Piper Diagram of Water Soluble-Salts